**d**Collection

工學碩士 學位論文

# 영향계수법을 이용한 아라온호의 국부 빙하중 산정 기법에 관한 연구

A Study on the Calculation Method of Local Ice Loads
for the IBRV ARAON using Influence Coefficient Method
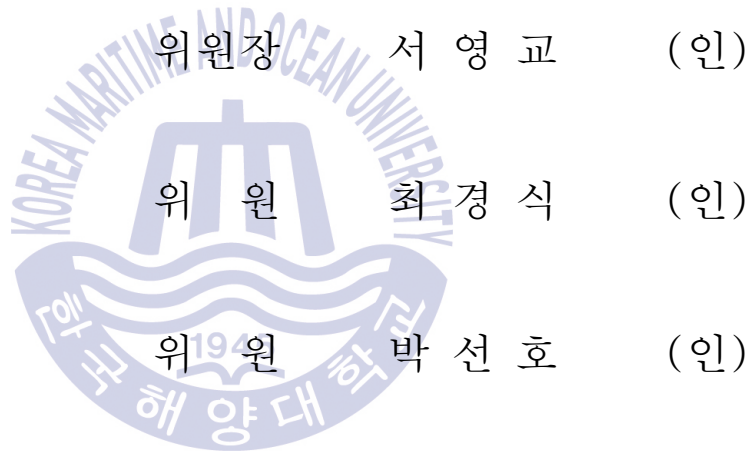
指導教授 崔 慶 植

2017年 2月

韓國海洋대학교 海洋科學技術專門大學院

海洋科學技術融合學科
閔 正 基

本 論文을 閔正基의 工學碩士 學位論文으로 認准함.

위원장    서 영 교    (인)

위  원    최 경 식    (인)

위  원    박 선 호    (인)

2016년  12월  23일

한국해양대학교  해양과학기술전문대학원

# Contents

# List of Tables

# List of Figures

# A Study on the Calculation Method of Local Ice Loads for the IBRV ARAON using Influence Coefficient Method

Min, Jung Ki

Department of Convergence Study on the Ocean Science and Technology
*Graduate School of Korea Maritime and Ocean University*

## Abstract

Ice load is one of the most important design factors for icebreaking vessels operating in ice-covered seas. In order to estimate the ice loads acting on ship hull, field measurement of ice pressures and the analysis of recorded data from ice trials are necessary. So far, few methods have been proposed to directly measure the ice loads on ship hull. This thesis focuses on the estimation of local ice loads exerted from ship-ice interaction processes. The Korean IBRV ARAON was used to perform field ice trials during her 2015 Arctic voyage. During ARAON's general ice transit, recorded data from both strain gauges on the inner hull shell plating and those installed on the transverse frames of the ARAON were analyzed to calculate ice loads. In this thesis, local ice loads estimated from the analysis of shear strain data on the side frames were compared to that from shell plating

pressures calculated by using an influence coefficient method. As a result, an alternate method of estimating local ice loads from shear strain measurement is recommended.

KEY WORDS: IBRV ARAON 쇄빙연구선 아라온; Strain gauge 스트레인게이지; Load inverse estimation method 하중 역추정 방법; Influence coefficient method 영향 계수법; Shear force 전단력;

# 1. Introduction

Over the past years, there has been a period of high oil prices due to the expansion of global economy. This trend has become a driving force for the development of resources in the polar regions. As shown in Fig. 1-1, it is estimated that Arctic offshore areas, including offshore Alaska, northern Canada and Siberia, have 30% of estimated world offshore oil and gas reserves.
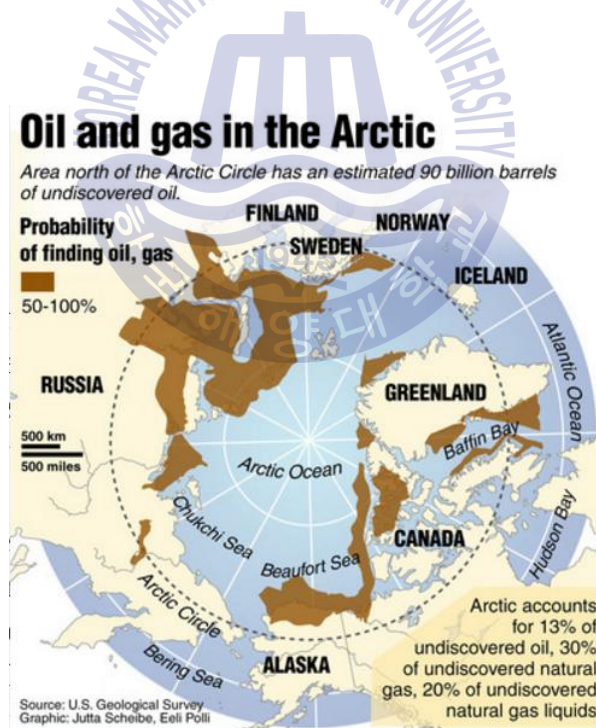


**Fig. 1-1** Oil and gas reserves in the Arctic region (USGS, 2008)

Icebreaking vessels in polar waters are subjected to various environmental loads such as wave loads and slamming forces, however the largest one that acts on the ship hull is the ice loads. In order to accurately estimate the ice loads, large amount of field data from ice trials have been gathered by several northern countries and the procedures for estimating the ice loads from the measured raw data have been studied in various ways. However, so far, few methods have been proposed to directly measure and to analyze the ice loads on ship hull. According to the contact area between hull and ice, ice loads acting on ships can be divided into two categories: global ice load and local ice load. The global ice load can be referred as the load in the sense of longitudinal strength of the hull, hull motion or vibration. On the other hand, local ice load is the load on local shell plating and surrounding members resulting in deformation and damage (Choi and Jeong, 2008).

This thesis focuses on the estimation of the local ice loads acting on the shell plating by using strain gauges installed on the hull of the icebreaking research vessel, ARAON. In order to estimate the ice loads, currently two approaches are possible. One method is a direct measurement of ice-structure interaction from the full-scale test in ice sea and the other method is a model test in ice tank basin and later expanding the result to full-scale situation. The more preferable method is to perform the full-scale ice trials, but it costs a lot of time and human labor. So far, there have been five ice field measurements in 2010, 2011, 2012, 2013 and 2015 in the Antarctic and Arctic seas using the Korean IBRV ARAON. In the beginning of the series of ice loading studies, the strain gauge measurements were not enough to produce correct relationship between structural response and ice loads because of the lack of the interpretation techniques. Since the ice trials in 2012, previous misinterpretation and insufficient apparatus has been

Collection @ kmou

supplemented and therefore a systematic analysis of measured strain data could be reached to produce better ice load estimation.

In this thesis, first, the attachment directions and types of strain gauges are discussed. A most accurate method to measure the deformation of shell platings is to use the 3-axis rosette strain gauges and then von Mises equivalent stress can be calculated from the measured strains in three directions. Ice loads acting on the hull are estimated from the equivalent stresses. In 2010 Arctic ice trials conducted by Korean researchers, single gauges and rosette gauges were used at the same time. According to the published results (Lee et al., 2013), different calculating schemes were used for the single gauges and rosette gauges. For single gauges, stresses are calculated directly by 1-dim. Hooke's law, however for the rosette gauges, von Mises equivalent stresses are calculated by 2-dim. analysis. Since it has been confirmed that there were no significant differences between two calculation schemes, i.e., using von Mises equivalent stress for the 3-axis rosette gauges and uniaxial stress using 1-dim. Hooke's law in 2010 ice trials. Because of this, only single gauges were used for the measurement during 2013 and 2015 ice trials. However, the analysis of strain gauge data from 2012 Antarctic ice trials showed that there might be a considerable difference between two calculation schemes, and therefore a revised calculation scheme is needed to correctly analyze 2015 Arctic data from where only single gauges were used.

Next in this thesis, the influence coefficient method is discussed. Influence coefficient method is the basic tool for calculating ice pressures acting on hull plating from ship hull stresses and the influence coefficients obtained by finite element analysis of hull plating are sensitive to the arrangement of strain gauges on hull plating. For the appropriate selection of influence coefficients,

a statistical analysis of strain data and a simple experiment were carried out.

    The goal of this study is the estimation of local ice loads exerted from ship-ice interaction processes during 2015 Arctic voyage of the IBRV ARAON. During ARAON's general ice transit, recorded data from both strain gauges on the inner shell  plating and those installed on the transverse frames of the ARAON were analyzed to calculate ice loads. In this thesis, local ice loads estimated from the analysis of shear strain data on the side frames were compared to that from shell plating pressures calculated by using an influence coefficient method. As a result, an alternate method of estimating local ice loads from shear strain measurement is recommended in the conclusions.

# 2. Strain gauge data analysis and influence coefficient method

## 2.1 Strain gauge measurement

The most commonly used device to measure strains is the strain gauge. Strain gauge adopts the concept of electrical resistance change in proportion to the deformation level of the object. Constantan, Nichrome, Karma and other metal alloys are used for the strain gauges depending on specific application. Constantan, which is an alloy of copper and nickel, is mostly used and its thickness is about $5\mu$m.

The shape of the metal strain gauge is composed of a microfiber wire or metal foil arranged in a lattice manner, which measures the amount of deformation of the metal wire or foil in the horizontal direction. The schematic form of the strain gauge is shown in Fig. 2-1 and it is attached directly to the surface of the object to be measured. Commercial strain gauges have resistance values of $30\Omega$ to $3000\Omega$, and the most commonly used ones are $120\Omega$, $350\Omega$ and $1000\Omega$.
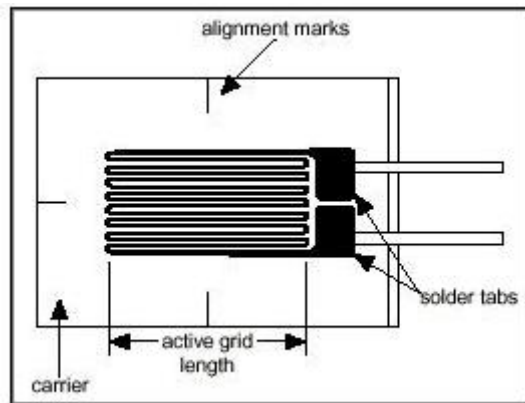
**Fig. 2-1** Strain gauge

Strain gauges can be categorized as 1-axis gauge (single gauge), 2-axis gauge (rosette gauge with 2 measuring grids) and 3-axis gauge (rosette gauge with 3 measuring grids) depending on the direction to be measured. The use of 1-axis gauge is cheaper than others and the number of connecting channels is small, so installation and data processing is easier. However, since only one direction of strain is measured, deformation in a two-dimensional plane is not more accurate than a two-axis or three-axis gauges. On the other hand, the 3-axis gauge is more costly, but it is most desirable to measure the direction and magnitude of principal stresses, such as estimating the ice loads acting on the shell plating. The type of the 3-axis gauge is also different when the direction of the strain axis is $0°$, $45°$, $90°$ and $0°$, $60°$, $120°$, respectively.

Fig. 2-2 Measurement and processing procedures of strain gauge data

When structure is deformed, the strain gauge attached to the surface changes the resistance value, and the strain is electrically amplified to record the strain. The bridge box connects the strain gauge with the amplifier (DAQ), and can be connected in Half, Quarter or Full mode. MGC Plus used for the measurement of strain is a product of HBM of Germany, which receives analog strain signals as many as necessary according to strain gauge type and connection method and stores them as digital data. The collected data is converted into various results such as strain and equivalent stress through the Catman Easy Program. Fig. 2-2 shows the procedure for processing strain gauge data.

## 2.2 Comparison of single gauge and rosette gauge

As mentioned above, there were five measurements of the field ice trial using icebreaking research vessel ARAON. Among them, a total of four experiments were carried out with strain gauges to measure hull strain: the Arctic in 2010, the Antarctic in 2012, the Arctic in 2013, the Arctic in 2015. For each field ice trial, the location and number of the strain gauge, and the type of strain gauge were slightly different. For this reason, it was not easy to compare the measured data values with each other. Furthermore, the definition of the stress value calculated from the measured data was not used equally, thereby causing confusion in the interpretation of the measurement data. Therefore, it is necessary to compare the strain gauge data measured in the field ice trial with each other in order to accurately estimate the ice load acting on the icebreaker. In this study, the difference between the method of using single gauge and rosette gauge installed in each field ice trial and the calculation method of stress are explained.

The method of calculating the stress generated on the shell plating by using the strain measured from the strain gauge installed on the inner shell of the hull is as follows.

$$\text{EX} : \quad \sigma_x = E \times \epsilon_x \tag{1}$$

$$\text{SSX} : \quad \sigma_1 = \frac{(\epsilon_1 + \mu\epsilon_2)E}{1-\mu^2}, \quad \sigma_2 = \frac{(\epsilon_2 + \mu\epsilon_1)E}{1-\mu^2} \tag{2}$$

$$\text{ES} : \quad \sigma_v = \sqrt{\sigma_1^2 + \sigma_2^2 - \sigma_1\sigma_2} \tag{3}$$

where $\epsilon_x$ is the measured deformation in the x-axis direction. E is the modulus of elasticity, and $\mu$ is the Poisson's ratio. $\epsilon_1$ and $\epsilon_2$ are the principal strains, and $\sigma_1$ and $\sigma_2$ are the principal stresses, respectively.

Eq.(1) is the uniaxial Hooke's law in which the strain is proportional to the stress in the elastic limit. So far, the stresses calculated when a single gauge is installed are used in this way. The reason why the deformation in the y-axis direction is not considered is that deformation in the fore-aft direction, that is, in the x-axis, is most affected in determining the stress in the hull plating of the ship. Eq.(2) is an equation for calculating the principal stress in the orthogonal direction in the plane problem, which is also used as a process of calculating the equivalent stress ES in Eq.(3). Eq.(3) is called the von Mises equivalent stress and is a general method of calculating stress using the strain measured on a 3-axis gauge.

In fact, when the measurement results of the rosette gauge(R3) installed in the 2010 Arctic ice trials are compared, it was confirmed that the directions of the principal strain alternately appeared around 180° and 0° around the x axis (i.e., fore-aft direction). The maximum and minimum values of the principal strain were similar to the maximum and minimum values of the measured strain in x-direction, respectively. Similarly, since the direction of principal stress is near 180° and 0°, the x-direction stress(EX) and the maximum principal stress(SSX) are relatively well matched. However, this judgment may not be appropriate in some cases especially in larger loading situations, as frequently seen in 2012 Antarctic ice trials. As an example, Fig. 2-3 shows the stress value of the L1 gauge in the official test (No.5 data set) recorded in the 2012 Antarctic ice trial using a rosette gauge. Overall, the calculation results show that the ES is larger than EX, and the difference is larger as the impact load is larger. In addition, EX shown in the lower circle is the calculated value of the negative stress value which can not be obtained by the ES calculation.
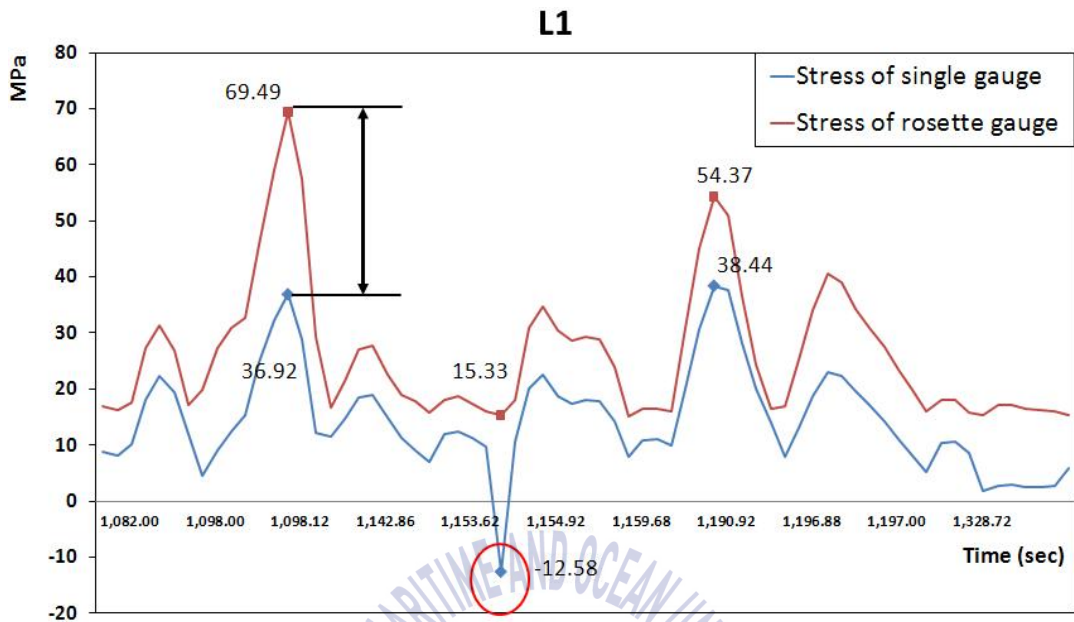
Fig. 2-3 Comparison of ES and EX calculated from rosette gauge L1 at the time of 2012 Antarctic ice trials
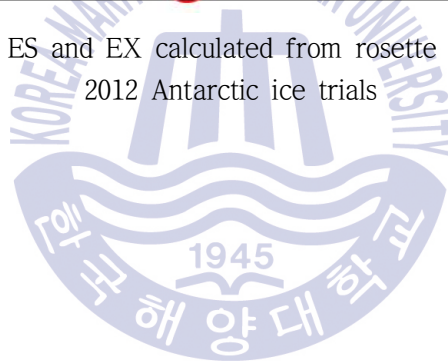
For this reason, in this study, although a single gauge was actually installed, a new scheme was proposed to derive a value as close as possible to the estimated load if a 3-axis gauge was installed. The use of only one axis gauge means that only the fore-aft direction, that is, the strain in the x-direction, is considered, and the y-direction and the other direction (45°) are not considered. In other words, the strain in the remaining directions except for the x direction is processed as zero. The calculation method is as follows. The strain corresponding to $\epsilon_A$ is used in the strain $\epsilon_A, \epsilon_B, \epsilon_c$ in the x-, y-, and 45° directions measured in the rosette gauge, and the strain in the remaining two directions is assumed to be zero. And then applying the value of $\epsilon_A$ to the von Mises equivalent stress formula, the stress from the single gauge can be treated as data from the rosette gauge. In other words, it is a method to calculate the stress by using only the strain in one direction measured through the single gauge and substituting it into the von Mises equivalent stress formula of Eq.(3).

To verify the usefulness of the proposed stress calculation scheme, old strain data from the 2010 Arctic ice trials (official ice-breaking tests were conducted over August 4, 5, and 6) and data from the 2012 Antarctic ice trials (the strain data measured in two official ice-breaking tests on February 22 and March 4) were used. Fig. 2-4 and Fig. 2-5 show the strain data from the Arctic and Antarctic tests in 2010 and 2012, respectively. In the first row, R-1 means rosette gauge number 1. R2-1, R2-2, and R2-3 mean rosette gauge number 2 displayed in order of x, y, and 45 degrees directions respectively. S1 means single gauge number 1. At the time of 2010 Arctic test, a combination of single gauges and rosette gauges was used, however, only the data using 3-axis rosette gauges without any malfunctioning were analyzed for verification. In 2012 Antarctic test, only rosette gauges were installed in both port and starboard and in this study, only the data measured at the port side without gauge failure were analyzed.

Collection @ kmou

| Time - defa | R1-1 CH=4 | S1 CH=5 | S2 CH=6 | R2-1 CH=7 | R2-2 CH=8 | R2-3 CH=9 | R3-1 CH=10 | R3-2 |
|---|---|---|---|---|---|---|---|---|
| 0 | 0.15833 | 0.37917 | -0.025 | 0.325 | 0.18333 | 0.05 | 0.25833 | 0 |
| 0.01 | 0.35 | 0.325 | -0.03333 | 0.60833 | 0.03333 | -0.20833 | 0.125 | -0 |
| 0.02 | 0.26667 | 0.38333 | -0.02083 | 0.73333 | -0.2 | -0.24167 | -0.05833 | |
| 0.03 | 0.275 | 0.42917 | -0.02917 | 0.675 | -0.15 | -0.19167 | -0.06667 | -0 |
| 0.04 | 0.40833 | 0.39167 | 0.05 | 0.78333 | -0.15833 | -0.23333 | -0.16667 | |
| 0.05 | 0.56667 | 0.32083 | 0.0125 | 0.83333 | -0.15 | -0.2 | -0.31667 | |
| 0.06 | 0.48333 | 0.28333 | -0.04583 | 0.83333 | -0.16667 | -0.29167 | -0.36667 | -0 |
| 0.07 | 0.33333 | 0.23333 | -0.1125 | 0.71667 | -0.2 | -0.24167 | -0.40833 | -0 |
| 0.08 | 0.375 | 0.22083 | -0.09583 | 0.78333 | -0.175 | -0.2 | -0.3 | -0 |

Fig. 2-4 Strain raw data from 2010 Arctic tests

| Time - det | L1-1 | L1-2 | L1-3 | L2-1 | L2-2 | L2-3 | L3-1 | L3-2 |
|---|---|---|---|---|---|---|---|---|
| | A | B | C | D | E | F | G | H |
| 0 | -0.09167 | 0.266667 | 0.025 | 0.791667 | 0.575 | 0.241667 | 0.041667 | 0.20 |
| 0.02 | -0.15 | 0.108333 | -0.13333 | 0.425 | 0.491667 | 0.241667 | 0.2 | 0.14 |
| 0.04 | -0.13333 | 0.133333 | -0.05 | 0.391667 | 0.458333 | 0.266667 | 0.208333 | 0.15 |
| 0.06 | -0.06667 | 0.233333 | -0.18333 | 0.525 | 0.525 | 0.291667 | 0.266667 | |
| 0.08 | -0.08333 | 0.191667 | -0.24167 | 0.575 | 0.558333 | 0.375 | 0.3 | |
| 0.1 | 0.008333 | 0.066667 | -0.51667 | 0.266667 | 0.491667 | 0.3 | 0.2 | 0.06 |
| 0.12 | 0.033333 | -0.04167 | -0.74167 | 0.008333 | 0.366667 | 0.316667 | 0.225 | 0.18 |
| 0.14 | 0.016667 | -0.10833 | -0.725 | -0.00833 | 0.425 | 0.283333 | 0.208333 | 0.34 |
| 0.16 | 0.15 | 0.06667 | -0.73333 | 0.00833 | 0.241667 | 0.266667 | 0.133333 | |

Fig. 2-5 Strain raw data from 2012 Antarctic tests

Stresses were calculated in three different ways, including the method presented here, using the strain data measured in 2010 and 2012. The first calculation scheme assumed that a 3-axis gauge is actually installed and only the x-direction strain measured in the gauge is applied to Hooke's law to calculate the stress(EX). The second scheme is to calculate the stress(ES1) using the von Mises equivalent stress formula, assuming that the strain except the x-direction is zero. The third scheme is to calculate the stress(ES) by using actual strains in all directions in the von Mises equivalent stress formula. Fig. 2-6 show directions of the strains that are used to obtain relevant stresses.

- 11 -
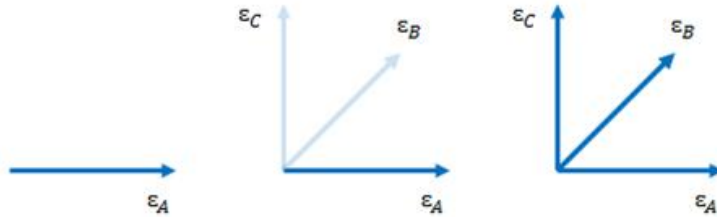
**Fig. 2-6** Strain directions in the stress calculation. From left, (a) EX (b) ES1 (c) ES

The calculated stresses were arranged in five levels; 5MPa or lower, 5~10MPa, 10~15MPa, 15~20MPa, and 20MPa or higher based on ES values. The difference between ES values and EX values calculated by first scheme was averaged. Also the difference between ES1 values calculated by second scheme and ES values by third scheme were averaged. The results are summarized in Fig. 2-8 and Table 2-1 to 2-4.

| | |
|---|---|
| 1. 2010_5Mpa or less data (Ex vs ES1 vs ES) | 1. 2012_5Mpa or less data (Ex vs ES1 vs ES) |
| 2. 2010_5~10Mpa data (Ex vs ES1 vs ES) | 2. 2012_5~10Mpa data (Ex vs ES1 vs ES) |
| 3. 2010_10~15Mpa data (Ex vs ES1 vs ES) | 3. 2012_10~15Mpa data (Ex vs ES1 vs ES) |
| 4. 2010_15~20MPa data (Ex vs ES1 vs ES) | 4. 2012_15~20MPa data (Ex vs ES1 vs ES) |
| 5. 2010_more than 20MPa data (Ex vs ES1 vs ES) | 5. 2012_more than 20Mpa data (Ex vs ES1 vs ES) |
| 6. 2010_result | 6. 2012_result |
| 2010-08-04_Run2 rosette gauge von stress | No.05_official rosette gauge von stress |
| 2010-08-04_Run2 single gauge Hooke's Law | No.05_official single gauge Hooke's Law |
| 2010-08-04_Run2 single gauge von stress | No.05_official single gauge von stress |
| 2010-08-04_Run2 | No.05_official |
| 2010-08-05_Run3 rosette gauge von stress | No.20_official rosette gauge von stress |
| 2010-08-05_Run3 single gauge Hooke's Law | No.20_official single gauge Hooke's Law |
| 2010-08-05_Run3 single gauge von stress | No.20_official single gauge von stress |
| 2010-08-05_Run3 | No.20_official |

**Fig. 2-7** (A) 2010 Arctic test data (b) 2012 Antarctic test data

**Table 2-1** ES vs. EX (Average of differences)

| (unit : MPa) | < 5 MPa | 5~10 MPa | 10~15 MPa | 15~20 MPa | >= 20 MPa |
|---|---|---|---|---|---|
| 2010 Arctic | 0.88 | 3.22 | 3.22 | 4.67 | 4.75 |
| 2012 Antarctic | 1.16 | 1.97 | 5.10 | 7.30 | 12.0 |

**Table 2-2** ES vs. ES1 (Average of differences)

| (unit : MPa) | < 5 MPa | 5~10 MPa | 10~15 MPa | 15~20 MPa | >= 20 MPa |
|---|---|---|---|---|---|
| 2010 Arctic | 0.78 | 2.70 | 1.60 | 2.41 | −0.30 |
| 2012 Antarctic | 0.86 | 1.19 | 3.87 | 5.48 | 8.65 |

**Table 2-3** ES vs. EX (Average of percentage)

| (unit : %) | < 5 MPa | 5~10 MPa | 10~15 MPa | 15~20 MPa | >= 20 MPa |
|---|---|---|---|---|---|
| 2010 Arctic | 42.11 | 45.04 | 73.76 | 72.59 | 83.00 |
| 2012 Antarctic | 56.53 | 68.47 | 57.00 | 57.65 | 59.90 |

**Table 2-4** ES vs. ES1 (Average of percentage)

| (unit : %) | < 5 MPa | 5~10 Mpa | 10~15 MPa | 15~20 MPa | >= 20 MPa |
|---|---|---|---|---|---|
| 2010 Arctic | 49.79 | 53.25 | 87.20 | 85.82 | 98.13 |
| 2012 Antarctic | 66.84 | 80.95 | 67.40 | 68.16 | 70.82 |
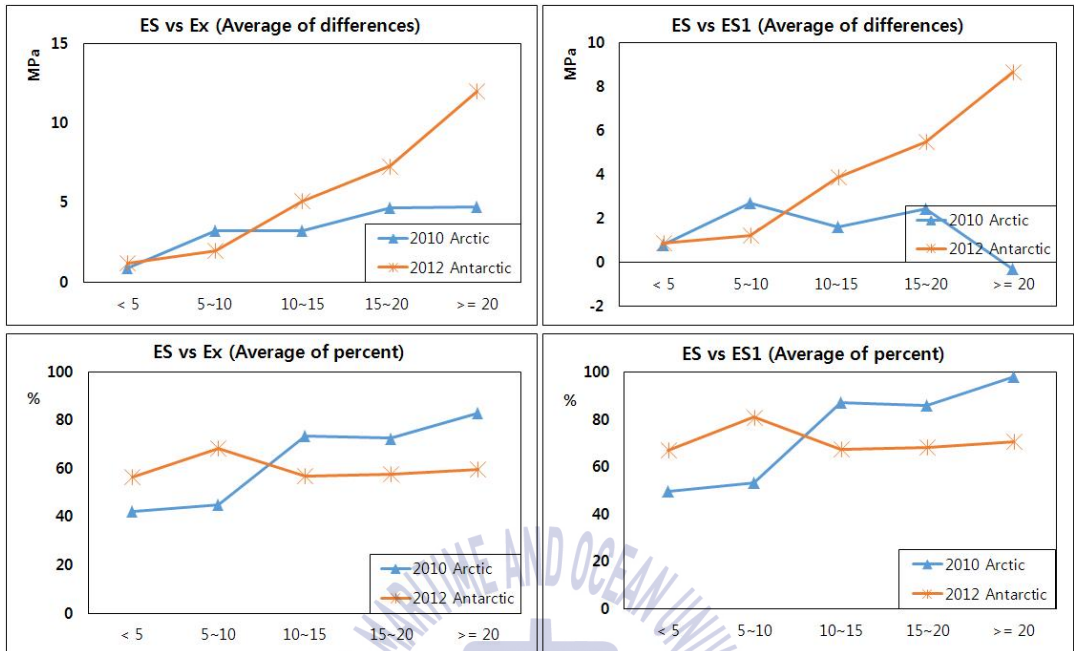
**Fig 2-8** Difference between ES and EX according to calculation schemes

As shown in Fig. 2-8, when the load acting on the hull is small (ice load in the Arctic is smaller than that in the Antarctic), the difference between EX and ES is not large. However, the larger the load, the larger the difference. The rapid increase in the difference between the two stresses can be found through 2012 Antarctic data. In 2010 Arctic data, the increase is slightly smaller, but the difference of load magnitude is steadily increasing. The graphs also show that ES1 is closer to ES than EX. Therefore, when a uniaxial strain gauge is installed, it is possible to obtain results closer to the actual stress by applying it to the von Mises equivalent stress formula instead of simple Hooke's law. When the Poisson ratio is 0.3, the ratio EX/ES1 is approximately 1.18.

## 2.3 Influence coefficient method

The technique for direct calculation of external loads acting on structure through the strain gauge measurement is not simple. In general, indirect estimation of loads through the complicated analysis of measured strain data can be used. Influence coefficient method is one of those indirect estimation techniques in consideration of structural deformation and measurement. Fig. 2-9 shows schematic diagram of load estimation procedures involved in the influence coefficient method.
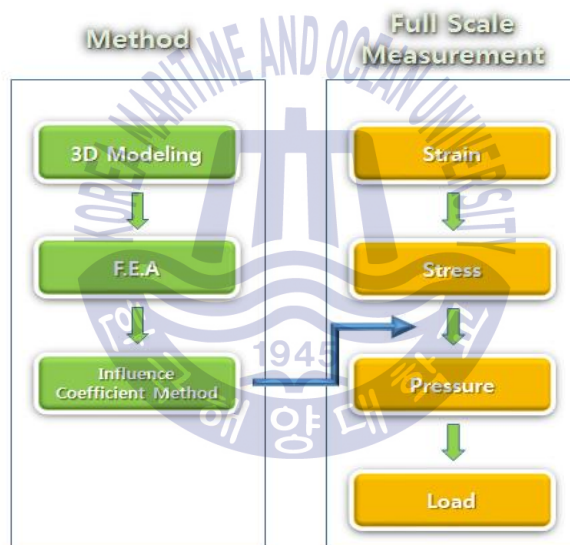


**Fig. 2-9** Outline of inversion technique using full scale measurement data and influence coefficient method

n this thesis, the relationship between hull stresses and pressures acting on the hull plating is derived by using the influence coefficient matrix, which is usually constructed from finite analysis of the structure involved. As shown in Fig. 2-10, a partial structure of the bow section of the IBRV ARAON is

selected for the finite element analysis using commercial FE software PATRAN. The size of shell plating covered by each strain gauge is selected as $800 \times 500\,mm$ and unit pressure is applied to each element to obtain influence coefficient matrix.
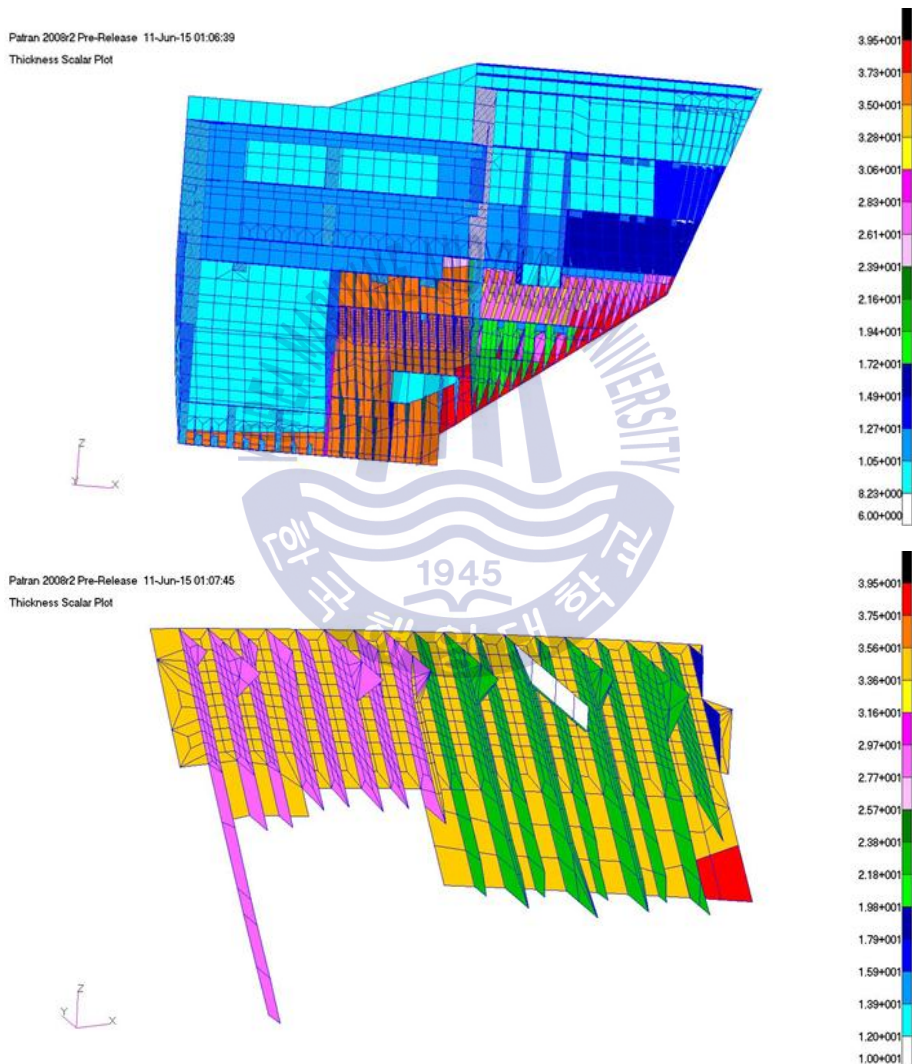


**Fig. 2-10** Structural analysis model for the bow section of the ARAON for interpretation of 2015 Arctic test data

Fig. 2-11 and 2-12 show the strain gauge arrays for the 2010 Arctic field ice trial and the 2012 Antarctic ice trials, respectively. For example, in the case of 2012 Antarctic, the influence coefficient matrix consists of $[11 \times 11]$ elements to match the arrangement of attached gauges. In Fig. 2-13, $[C]$ represents the influence coefficient matrix and an inverse matrix $[C]^{-1}$ becomes an influence coefficient matrix of the equivalent hull stresses, that is connected to external ice pressures.
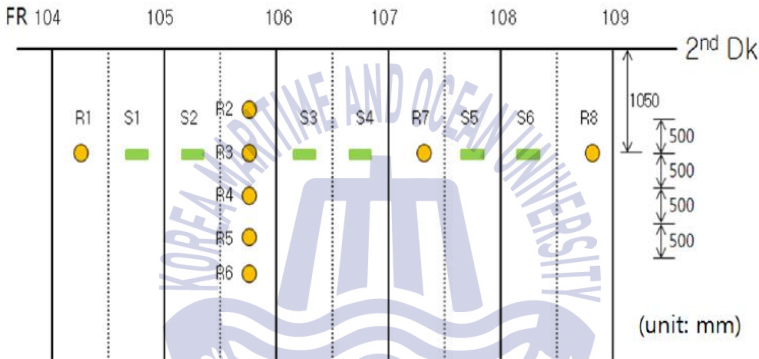


Fig. 2-11 Strain gauge arrays for 2010 Arctic ice trials
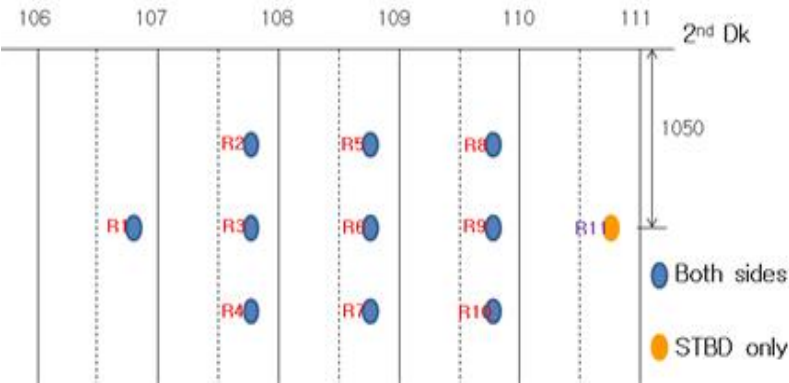


Fig. 2-12 Strain gauge arrays for 2012 Antarctic ice trials

- 17 -

$$\begin{bmatrix} \sigma_1 \\ \sigma_2 \\ \sigma_3 \\ \cdot \\ \cdot \\ \cdot \\ \sigma_{11} \end{bmatrix} = [c] \begin{bmatrix} P_1 \\ P_2 \\ P_3 \\ \cdot \\ \cdot \\ \cdot \\ P_{11} \end{bmatrix} \implies \begin{bmatrix} P_1 \\ P_2 \\ P_3 \\ \cdot \\ \cdot \\ \cdot \\ P_{11} \end{bmatrix} = [c]^{-1} \begin{bmatrix} \sigma_1 \\ \sigma_2 \\ \sigma_3 \\ \cdot \\ \cdot \\ \cdot \\ \sigma_{11} \end{bmatrix}$$

Fig. 2-13 Relationship between the hull stresses and external ice pressures

As the size of influence coefficient matrix increases, the estimated load is closer to the actual value. This means that the larger the number of gauges installed on the shell plate, the larger the size of influence coefficient matrix. However, if the load is applied to some area where gauges are not installed, it is rather difficult to deal with the problem in normal way to interpret influence coefficient method. In 2015 Arctic ice trials, strain gauges were installed between Fr.102 and Fr.110 under $2^{nd}$ deck where the ice interacts mostly. Fig. 2-14 and Fig. 2-15 show the strain gauge arrangements during 2015 Arctic ice trials and the influence coefficient matrices are shown in Tables 2-5 and Table 2-6. In Fig. 2-14, single gauges were installed in the dotted area, and the area marked with $\times$ is the rosette gauge installed in the frames. On the starboard side, only half the number of gauges in the port side was installed. There were single gauges and 10 rosette gauges installed on the port, and 12 single gauges and 4 rosette gauges were installed on starboard side. A total of 78 channels can be recorded at the same time.

The number of single gauges installed inside the shell plating was 24 and unit pressure was imposed on the area occupied by each gauge. Then the process of obtaining the equivalent stresses of all remaining parts can be

repeated 24 times to construct the influence coefficient matrix $[24 \times 24]$. Since ARAON's left and right side structures are identical, size of $[12 \times 12]$ matrix among the $[24 \times 24]$ influence coefficient matrix of starboard side can be used for the port side. Influence coefficient matrix was not calculated for the frame area where the rosette gauge installed.



**Fig. 2-14** Layout of strain gauges on the hull panel of the IBRV ARAON during 2015 Arctic ice trials (port side)



**Fig. 2-15** Layout of strain gauges on the hull panel of the IBRV ARAON during 2015 Arctic ice trials (starboard side)

**Table 2-5** Influence coefficient matrix for port side hull plating $[24 \times 24]$

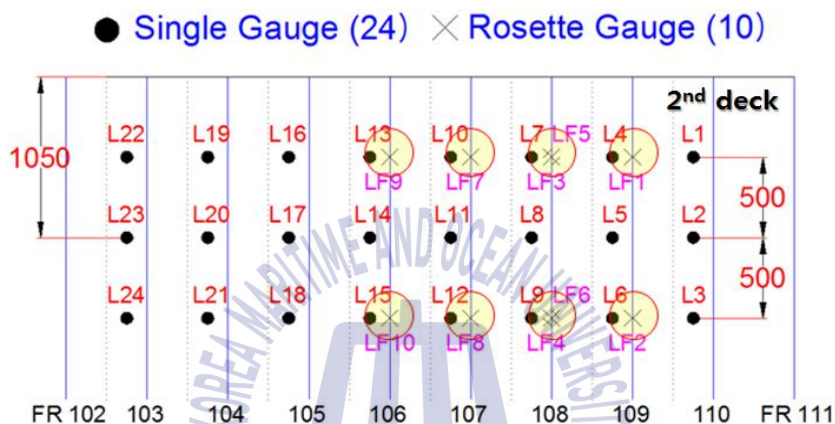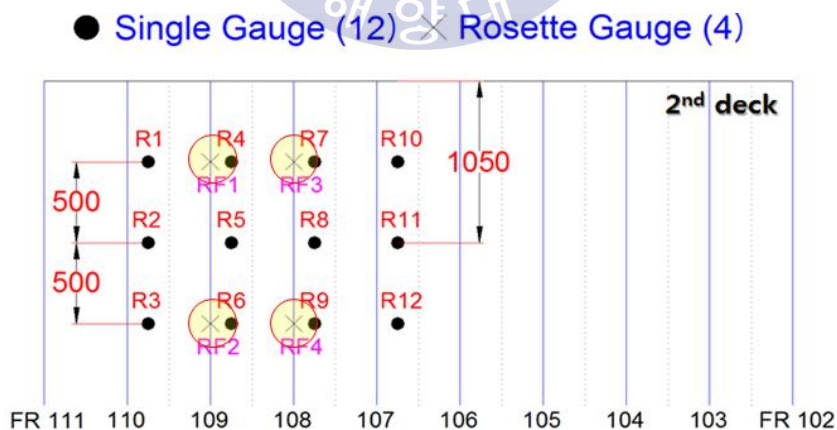| | L1 | L2 | L3 | L4 | L5 | L6 | L7 | L8 | L9 | L10 | L11 | L12 | L13 | L14 | L15 | L16 | L17 | L18 | L19 | L20 | L21 | L22 | L23 | L24 |
|---|---|---|---|---|---|---|---|---|---|---|---|---|---|---|---|---|---|---|---|---|---|---|---|---|
| L1 | 40.927 | 9.085 | 3.538 | 2.508 | 2.959 | 2.895 | 1.454 | 1.151 | 0.848 | 1.201 | 1.088 | 0.920 | 1.048 | 0.937 | 0.839 | 0.928 | 0.852 | 0.782 | 0.813 | 0.778 | 0.732 | 0.729 | 0.711 | 0.678 |
| L2 | 8.155 | 45.456 | 12.481 | 2.896 | 4.508 | 4.549 | 1.603 | 1.399 | 1.058 | 1.307 | 1.253 | 1.111 | 1.126 | 1.045 | 0.957 | 0.983 | 0.924 | 0.866 | 0.857 | 0.830 | 0.791 | 0.764 | 0.752 | 0.725 |
| L3 | 2.557 | 11.988 | 47.815 | 2.398 | 4.608 | 5.348 | 1.565 | 1.489 | 1.292 | 1.312 | 1.317 | 1.231 | 1.149 | 1.101 | 1.039 | 1.003 | 0.963 | 0.922 | 0.876 | 0.860 | 0.831 | 0.782 | 0.776 | 0.756 |
| L4 | 0.749 | 1.290 | 1.528 | 41.740 | 9.905 | 4.101 | 2.244 | 2.973 | 3.418 | 1.568 | 1.326 | 1.040 | 1.327 | 1.149 | 0.980 | 1.148 | 1.021 | 0.902 | 0.967 | 0.904 | 0.824 | 0.835 | 0.797 | 0.739 |
| L5 | 0.835 | 1.497 | 2.666 | 8.774 | 47.046 | 13.645 | 2.733 | 4.611 | 5.301 | 1.677 | 1.588 | 1.291 | 1.422 | 1.306 | 1.152 | 1.220 | 1.122 | 1.017 | 1.020 | 0.972 | 0.898 | 0.874 | 0.845 | 0.794 |
| L6 | 1.400 | 2.061 | 2.893 | 3.587 | 14.039 | 48.862 | 2.316 | 4.878 | 6.183 | 1.600 | 1.673 | 1.527 | 1.414 | 1.363 | 1.264 | 1.228 | 1.164 | 1.089 | 1.031 | 1.002 | 0.943 | 0.886 | 0.867 | 0.826 |
| L7 | 0.775 | 0.568 | 0.416 | 0.688 | 1.440 | 1.395 | 42.176 | 10.387 | 4.408 | 2.993 | 3.636 | 3.252 | 1.706 | 1.344 | 1.013 | 1.422 | 1.222 | 1.023 | 1.154 | 1.048 | 0.914 | 0.960 | 0.894 | 0.802 |
| L8 | 0.866 | 0.691 | 0.547 | 0.983 | 1.550 | 2.243 | 9.024 | 46.838 | 13.350 | 3.356 | 4.912 | 4.713 | 1.831 | 1.606 | 1.224 | 1.550 | 1.402 | 1.223 | 1.245 | 1.163 | 1.031 | 1.026 | 0.972 | 0.887 |
| L9 | 0.858 | 0.738 | 0.628 | 1.512 | 2.008 | 2.414 | 3.648 | 13.324 | 48.323 | 2.709 | 4.870 | 5.418 | 1.748 | 1.697 | 1.494 | 1.560 | 1.481 | 1.375 | 1.271 | 1.223 | 1.118 | 1.056 | 1.018 | 0.951 |
| L10 | 0.617 | 0.417 | 0.314 | 0.837 | 0.770 | 0.580 | 0.905 | 1.147 | 1.399 | 41.051 | 9.546 | 3.990 | 2.358 | 2.681 | 2.812 | 1.769 | 1.422 | 1.114 | 1.385 | 1.219 | 1.014 | 1.107 | 1.011 | 0.885 |
| L11 | 0.709 | 0.514 | 0.406 | 0.985 | 1.008 | 0.815 | 0.912 | 1.325 | 2.381 | 8.455 | 45.824 | 13.180 | 2.728 | 4.024 | 4.186 | 1.927 | 1.716 | 1.379 | 1.521 | 1.404 | 1.198 | 1.197 | 1.124 | 1.014 |
| L12 | 0.766 | 0.594 | 0.491 | 1.027 | 1.127 | 0.969 | 1.308 | 1.813 | 2.560 | 3.198 | 12.940 | 47.947 | 2.268 | 4.258 | 4.892 | 1.894 | 1.842 | 1.643 | 1.560 | 1.509 | 1.356 | 1.242 | 1.196 | 1.116 |
| L13 | 0.480 | 0.327 | 0.248 | 0.587 | 0.480 | 0.371 | 0.645 | 0.539 | 0.496 | 0.785 | 1.300 | 1.504 | 39.010 | 8.591 | 3.831 | 2.238 | 2.070 | 2.507 | 1.687 | 1.398 | 1.117 | 1.296 | 1.163 | 0.974 |
| L14 | 0.566 | 0.412 | 0.327 | 0.671 | 0.571 | 0.466 | 0.716 | 0.690 | 0.653 | 0.962 | 1.414 | 2.387 | 7.454 | 43.575 | 12.348 | 2.612 | 3.265 | 3.681 | 1.892 | 1.723 | 1.417 | 1.447 | 1.355 | 1.169 |
| L15 | 0.634 | 0.489 | 0.405 | 0.732 | 0.650 | 0.553 | 0.728 | 0.775 | 0.756 | 1.498 | 1.944 | 2.523 | 2.902 | 11.936 | 46.125 | 2.334 | 3.741 | 4.571 | 1.907 | 1.879 | 1.711 | 1.519 | 1.478 | 1.338 |
| L16 | 0.343 | 0.239 | 0.186 | 0.436 | 0.346 | 0.253 | 0.474 | 0.346 | 0.319 | 0.595 | 0.609 | 0.553 | 0.676 | 1.235 | 1.610 | 39.604 | 9.173 | 4.436 | 2.339 | 2.436 | 2.683 | 1.491 | 1.241 | 0.945 |
| L17 | 0.413 | 0.314 | 0.257 | 0.515 | 0.421 | 0.313 | 0.549 | 0.436 | 0.396 | 0.644 | 0.743 | 0.737 | 0.748 | 1.468 | 2.717 | 8.066 | 44.781 | 13.456 | 2.799 | 3.801 | 4.279 | 1.644 | 1.499 | 1.137 |
| L18 | 0.467 | 0.376 | 0.320 | 0.572 | 0.481 | 0.368 | 0.601 | 0.513 | 0.460 | 0.648 | 0.815 | 0.862 | 1.351 | 2.133 | 3.131 | 3.759 | 13.212 | 47.978 | 2.503 | 4.250 | 5.457 | 1.649 | 1.633 | 1.377 |
| L19 | 0.199 | 0.133 | 0.105 | 0.269 | 0.213 | 0.161 | 0.310 | 0.211 | 0.187 | 0.411 | 0.372 | 0.318 | 0.541 | 0.538 | 0.519 | 0.498 | 1.303 | 1.546 | 39.068 | 9.099 | 4.309 | 2.195 | 2.668 | 2.935 |
| L20 | 0.247 | 0.177 | 0.142 | 0.332 | 0.271 | 0.209 | 0.385 | 0.273 | 0.236 | 0.502 | 0.469 | 0.411 | 0.640 | 0.702 | 0.735 | 0.796 | 1.557 | 2.660 | 8.375 | 44.324 | 13.081 | 2.969 | 4.438 | 5.021 |
| L21 | 0.279 | 0.212 | 0.173 | 0.373 | 0.312 | 0.247 | 0.433 | 0.322 | 0.275 | 0.551 | 0.531 | 0.478 | 0.658 | 0.793 | 0.894 | 1.421 | 2.268 | 2.997 | 3.744 | 12.515 | 47.244 | 2.706 | 4.724 | 6.263 |
| L22 | 0.088 | 0.059 | 0.054 | 0.128 | 0.101 | 0.082 | 0.151 | 0.104 | 0.098 | 0.215 | 0.193 | 0.172 | 0.305 | 0.290 | 0.264 | 0.367 | 0.384 | 0.394 | 0.419 | 1.060 | 1.404 | 38.560 | 10.107 | 6.324 |
| L23 | 0.115 | 0.087 | 0.077 | 0.164 | 0.134 | 0.110 | 0.197 | 0.142 | 0.129 | 0.277 | 0.257 | 0.239 | 0.405 | 0.416 | 0.388 | 0.445 | 0.526 | 0.616 | 0.539 | 1.556 | 2.731 | 8.702 | 44.929 | 16.678 |
| L24 | 0.136 | 0.110 | 0.098 | 0.191 | 0.161 | 0.136 | 0.232 | 0.179 | 0.162 | 0.324 | 0.309 | 0.298 | 0.470 | 0.507 | 0.493 | 0.465 | 0.630 | 0.831 | 1.322 | 2.377 | 3.278 | 4.161 | 14.593 | 51.645 |

**Table 2-6** Influence coefficient matrix for starboard side hull plating $[12 \times 12]$

| | R1 | R2 | R3 | R4 | R5 | R6 | R7 | R8 | R9 | R10 | R11 | R12 |
|---|---|---|---|---|---|---|---|---|---|---|---|---|
| R1 | 40.927 | 9.085 | 3.538 | 2.508 | 2.959 | 2.895 | 1.454 | 1.151 | 0.848 | 1.201 | 1.088 | 0.920 |
| R2 | 8.155 | 45.456 | 12.481 | 2.896 | 4.508 | 4.549 | 1.603 | 1.399 | 1.058 | 1.307 | 1.253 | 1.111 |
| R3 | 2.557 | 11.988 | 47.815 | 2.398 | 4.608 | 5.348 | 1.565 | 1.489 | 1.292 | 1.312 | 1.317 | 1.231 |
| R4 | 0.749 | 1.290 | 1.528 | 41.740 | 9.905 | 4.101 | 2.244 | 2.973 | 3.418 | 1.568 | 1.326 | 1.040 |
| R5 | 0.835 | 1.497 | 2.666 | 8.774 | 47.046 | 13.645 | 2.733 | 4.611 | 5.301 | 1.677 | 1.588 | 1.291 |
| R6 | 1.400 | 2.061 | 2.893 | 3.587 | 14.039 | 48.862 | 2.316 | 4.878 | 6.183 | 1.600 | 1.673 | 1.527 |
| R7 | 0.775 | 0.568 | 0.416 | 0.688 | 1.440 | 1.395 | 42.176 | 10.387 | 4.408 | 2.993 | 3.636 | 3.252 |
| R8 | 0.866 | 0.691 | 0.547 | 0.983 | 1.550 | 2.243 | 9.024 | 46.838 | 13.350 | 3.356 | 4.912 | 4.713 |
| R9 | 0.858 | 0.738 | 0.628 | 1.512 | 2.008 | 2.414 | 3.648 | 13.324 | 48.323 | 2.709 | 4.870 | 5.418 |
| R10 | 0.617 | 0.417 | 0.314 | 0.837 | 0.770 | 0.580 | 0.905 | 1.147 | 1.399 | 41.051 | 9.546 | 3.990 |
| R11 | 0.709 | 0.514 | 0.406 | 0.985 | 1.008 | 0.815 | 0.912 | 1.325 | 2.381 | 8.455 | 45.824 | 13.180 |
| R12 | 0.766 | 0.594 | 0.491 | 1.027 | 1.127 | 0.969 | 1.308 | 1.813 | 2.560 | 3.198 | 12.940 | 47.947 |

Fig. 2-16 ARAON's 2015 Arctic field ice trial

## 2.4 Selection of influence coefficient matrix

There may be an unexpected situation when using strain gauges during the test. Because the strain gauges are very sensitive to ambient environment such as temperature or impact, it is often impossible to use them due to gauge failure. During the ice trials in the Arctic ice sea, 2015, the gauge #21, which was installed on the port side of ARAON's bow section, could not be used due to gauge failure. Therefore, unlike the other parts where the normal data was recorded, the strain of the shell plating part of that gauge could not recorded In order to overcome this kind of problem, alternate schemes to estimate ice loads considering gauge failure in some regions are tried in this study. The following two methods are related with modification of the influence coefficient matrix considering the failed part.

① Interpolation through statistical analysis of measured data

② Reduction of influence coefficient matrix by excluding stress data that comes from failed gauges

First, a statistical analysis with Pearson's correlation coefficient is applied to 2012 Antarctic data, Pearson's correlation coefficient is the covariance of two variables divided by the product of their standard deviations. If the correlation coefficient is 1 or -1, it means that two variables are related in completely positive or completely negative. A value of 0 means that the two variables are independent of each other. Generally, if the correlation coefficient is more than 0.4, it means that there is somewhat high correlation between two variables (Yang, 2012).

$$R = \frac{the \deg ree\,A}{the \deg ree\,B}$$

A is that x and y are mutually changed, and B is that x and y are mutually different. 2012 Antarctic strain data (No.1 to No.21 data sets) were converted to the equivalent stress and then filtered by 15MPa threshold. In No.13 data set, there were no higher stresses than 15MPa. No.17 and No.18 data sets were excluded because of gauge failure. Pearson's correlation coefficients for each gauge are shown in Table 2-7. Table 2-8 shows the correlation coefficients with adjacent gauges based on L6 gauge (located at the center of the installed gauges in the port side.

Table 2-7 Pearson's correlation coefficients between gauges

|  | L1 | L2 | L3 | L4 | L5 | L6 | L7 | L8 | L9 | L10 |
|---|---|---|---|---|---|---|---|---|---|---|
| L1 | 1 | 0.3008 | 0.2923 | 0.2694 | 0.1763 | 0.1575 | 0.1845 | 0.1647 | -0.0002 | -0.0200 |
| L2 | 0.3008 | 1 | 0.6083 | 0.3388 | 0.3521 | 0.2749 | 0.2601 | 0.3275 | -0.0008 | 0.0242 |
| L3 | 0.2923 | 0.6083 | 1 | 0.4727 | 0.2386 | 0.2526 | 0.2258 | 0.1993 | -0.0009 | 0.0138 |
| L4 | 0.2694 | 0.3388 | 0.4727 | 1 | 0.2140 | 0.2232 | 0.2999 | 0.2173 | 0.0000 | 0.0618 |
| L5 | 0.1763 | 0.3521 | 0.2386 | 0.2140 | 1 | 0.5340 | 0.2532 | 0.3202 | 0.0016 | 0.0489 |
| L6 | 0.1575 | 0.2749 | 0.2526 | 0.2232 | 0.5340 | 1 | 0.5058 | 0.2299 | 0.0013 | 0.0801 |
| L7 | 0.1845 | 0.2601 | 0.2258 | 0.2999 | 0.2532 | 0.5058 | 1 | 0.2153 | 0.0018 | 0.1707 |
| L8 | 0.1647 | 0.3275 | 0.1993 | 0.2173 | 0.3202 | 0.2299 | 0.2153 | 1 | 0.0013 | 0.0847 |
| L9 | -0.0002 | -0.0008 | -0.0009 | 0.0000 | 0.0016 | 0.0013 | 0.0018 | 0.0013 | 1 | 0.0008 |
| L10 | -0.0200 | 0.0242 | 0.0138 | 0.0618 | 0.0489 | 0.0801 | 0.1707 | 0.0847 | 0.0008 | 1 |

**Table 2-8** Pearson's correlation coefficients around L6 gauge

|  |  | L2 | 0.27487 | L5 | 0.53405 | L8 | 0.22990 |
|---|---|---|---|---|---|---|---|
| L1 | 0.15750 | L3 | 0.25263 | L6 | 1 | L9 | 0.00128 |
|  |  | L4 | 0.22321 | L7 | 0.50583 | L10 | 0.08009 |

From the statistical analysis using Pearson's correlation coefficients, some explanation can be drawn on the relationship between installed gauges. First, the correlation in the vertical gauge arrays is higher than that in the horizontal direction. If one or two strain gauges are in failure, then it is possible to estimate an actual load by interpolating strain values in the vertical direction. Second, although the correlation coefficient is larger than 0.5, the result explains that the ice load acting on one gauge have little influence on the other gauges (Kwon, et al., 2015) and this can be a basis for alternate scheme to calculate stresses by excluding gauges in failure.

The interpolation method can estimate the data value while maintaining the size of influence coefficient matrix. On the other hand, size of the matrix may be reduced according to the array of gauges. First, the loads are estimated using the measured strain gauge data. For this case, the stress of failed gauge is assumed to be zero. Secondly, a reduced matrix is used in the calculation process by excluding rows and columns corresponding to failed gauges.

The first method with zero stresses of failed gauges has been adopted to calculate the ice pressures in 2010 Arctic ice trials (Lee et al., 2013). To calculate pressures on shell plating as shown in Fig. 2-16, the influence coefficient matrix for nine sub-panels was extracted. However, stresses were only measured from five gauges (R2, S2, R3, S3, and R4). In this case, the influence coefficient matrix must be $9 \times 9$ array, and the number of actually measured stresses is 5, hence it is assumed that the stresses corresponding to remaining positions 1, 3, 7, and 9 are zero. The larger the size of influence coefficient matrix, the more accurate load can be obtained. Also, the larger the number of installed gauges, the larger the size of influence coefficient matrix. Since the number of installed gauges has a limitation, it is necessary to calculate the influence coefficient matrix assuming that stresses of sub-panels without gauges or without measured data is zero.
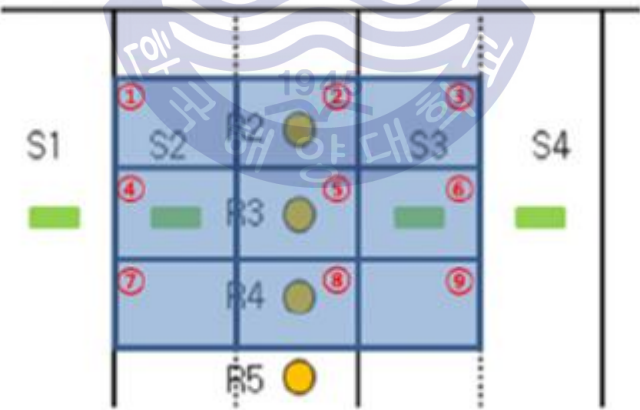


Fig. 2-17 Construction of the influence coefficient matrix for calculating ice pressures in 2010 Arctic ice trials (Lee et al., 2013)

On the other hand, the second method of using a reduced influence coefficient matrix can be applied to the cases when multiple gauges fail or when fewer gauges are installed than expected. Figure 2-17 shows an example. At the time of 2012 Antarctic ice trials, the array of gauges was entirely covered by the array of gauges installed for 2015 Arctic ice trials. Therefore, when ice pressures are to be obtained from the 2012 Antarctic data with a small number of gauge array, the total influence coefficient matrix can be used with a reduced size by deleting rows and columns corresponding to the part where the gauges were not installed.



**Total Influence coefficient matrix [24 X 24]**

**Reduced influence coefficient matrix [10 X 10]**

Calculate by reducing rows and columns.

$C_{Reduce}$

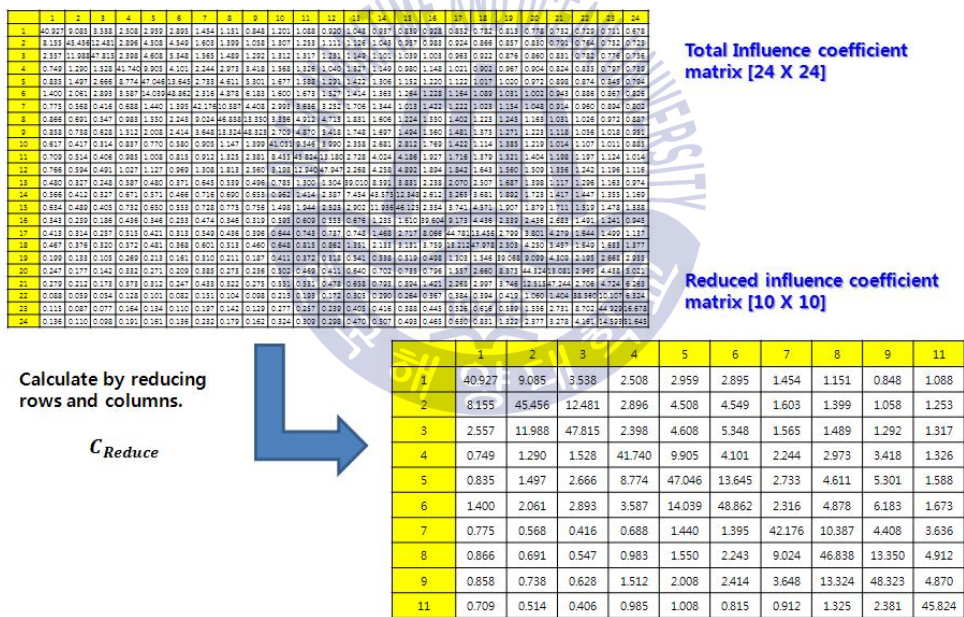| | 1 | 2 | 3 | 4 | 5 | 6 | 7 | 8 | 9 | 11 |
|---|---|---|---|---|---|---|---|---|---|---|
| 1 | 40.927 | 9.085 | 3.538 | 2.508 | 2.959 | 2.895 | 1.454 | 1.151 | 0.848 | 1.088 |
| 2 | 8.155 | 45.456 | 12.481 | 2.896 | 4.508 | 4.549 | 1.603 | 1.399 | 1.058 | 1.253 |
| 3 | 2.557 | 11.988 | 47.815 | 2.398 | 4.608 | 5.348 | 1.565 | 1.489 | 1.292 | 1.317 |
| 4 | 0.749 | 1.290 | 1.528 | 41.740 | 9.905 | 4.101 | 2.244 | 2.973 | 3.418 | 1.326 |
| 5 | 0.835 | 1.497 | 2.666 | 8.774 | 47.046 | 13.645 | 2.733 | 4.611 | 5.301 | 1.588 |
| 6 | 1.400 | 2.061 | 2.893 | 3.587 | 14.039 | 48.862 | 2.316 | 4.878 | 6.183 | 1.673 |
| 7 | 0.775 | 0.568 | 0.416 | 0.688 | 1.440 | 1.395 | 42.176 | 10.387 | 4.408 | 3.636 |
| 8 | 0.866 | 0.691 | 0.547 | 0.983 | 1.550 | 2.243 | 9.024 | 46.838 | 13.350 | 4.912 |
| 9 | 0.858 | 0.738 | 0.628 | 1.512 | 2.008 | 2.414 | 3.648 | 13.324 | 48.323 | 4.870 |
| 11 | 0.709 | 0.514 | 0.406 | 0.985 | 1.008 | 0.815 | 0.912 | 1.325 | 2.381 | 45.824 |

Fig. 2-18 Original influence coefficient matrix and reduced matrix for 2012 Antarctic ice trials

For comparison of two methods mentioned, in this study a simple experiment was carried out. Fig. 2-18 shows the rectangular plate model used for verification. A commercial finite element analysis program, ANSYS v13.0 is

- 26 -

used for the plate model as shown in Fig. 2-20. In the loading test, unit load, 1N is sequentially applied to the points ① to ⑨ where rosette gauges are attached. The equivalent stresses are calculated using measured deflections of the plate at each gauge point and $[9 \times 9]$ influence coefficient matrix is constructed as in Table 2-9.
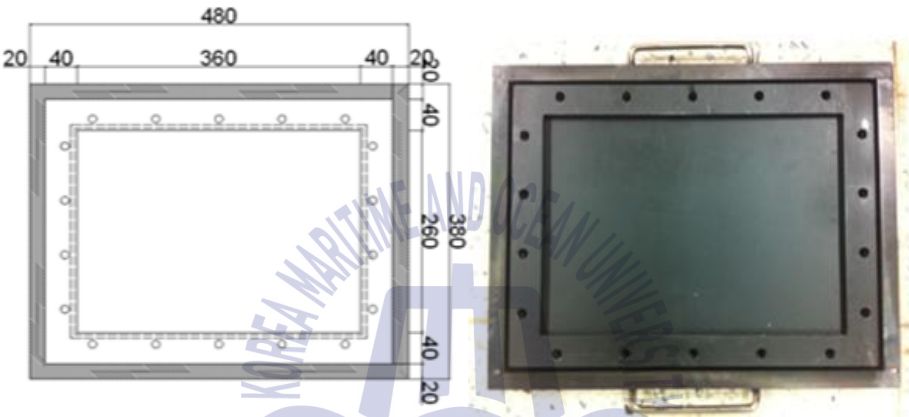


Fig. 2-19 Assembled plate model (Fixed on four sides)



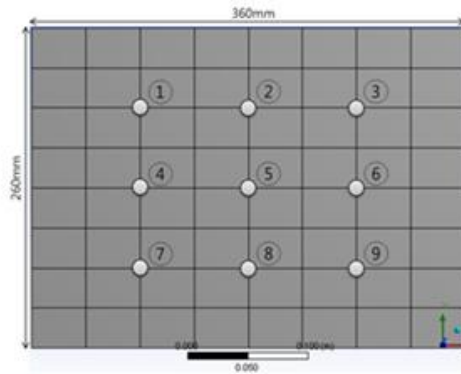Fig. 2-20 Simple loading test on the
plate model

**Fig. 2-21** Modeling with ANSYS FE program

**Table 2-9** Constructed influence coefficient matrix using ANSYS

| Influence coefficient matrix (unit : Pa) | | | | | | | | |
|--------|--------|--------|--------|--------|--------|--------|--------|--------|
| 268240 | 24679 | 5763.8 | 33984 | 31867 | 9529.2 | 12481 | 13450 | 4467.9 |
| 19323 | 329600 | 19323 | 20706 | 28610 | 20706 | 8077.4 | 10595 | 8077.4 |
| 5763.8 | 24679 | 268240 | 9529.2 | 31867 | 33984 | 4467.9 | 13450 | 12481 |
| 27683 | 16385 | 5123.4 | 290130 | 32080 | 9572.4 | 27683 | 16385 | 5123.4 |
| 14879 | 30404 | 14879 | 29372 | 364540 | 29372 | 14879 | 30404 | 14879 |
| 5123.4 | 16385 | 27683 | 9572.4 | 32080 | 290130 | 5123.4 | 16385 | 27683 |
| 12481 | 13450 | 4467.9 | 33984 | 31867 | 9529.2 | 268240 | 24679 | 5763.8 |
| 8077.4 | 10595 | 8077.4 | 20706 | 28610 | 20706 | 19323 | 329600 | 19323 |
| 4467.9 | 13450 | 12481 | 9529.2 | 31867 | 33984 | 5763.8 | 24679 | 268240 |

Size of the plate is 360mm×260mm and thickness, 3mm, elastic modulus, 245GPa made of stainless steel. The area covered by one gauge is 95mm× 65mm. Sampling rate is 50Hz and the same experiments were carried out four times. Here the equivalent stress is the average of the four measured values in 10 to 20 seconds after applying the point force as shown in Fig. 2-21.
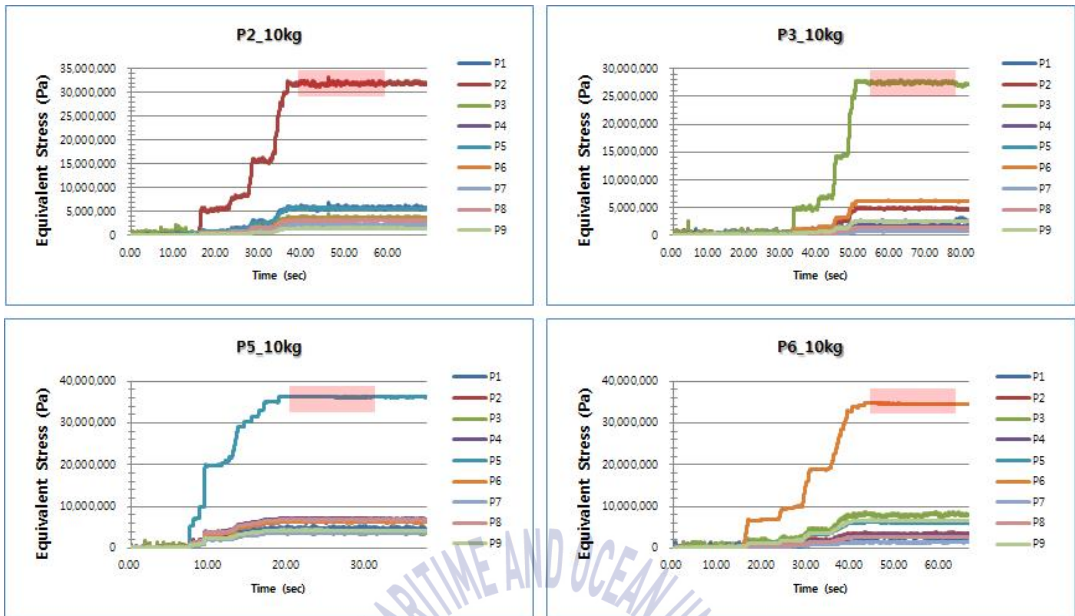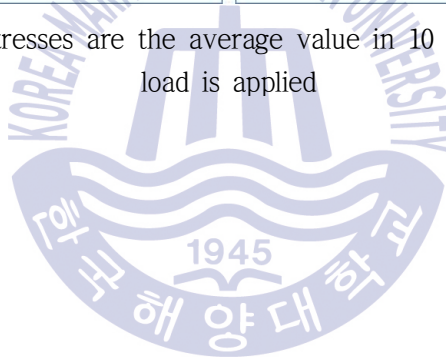
Collection @ kmou

Fig. 2-22 Equivalent stresses are the average value in 10 to 20 seconds after the load is applied

First method: measured stresses are shown in Table 2-10 assuming that stresses without gauges are zero.

(a) Calculated stresses at each point when all nine gauges are installed

(b) Assuming that a gauge is not installed at P2

(c) Assuming that gauges are not installed at P2, P4, P6, P8

(d) Assuming that the stresses of the remaining points except P1, P3, P7, and P9 are zero

Table 2-10 Measured stresses assuming that stresses without gauges are zero

| (unit : MPa) | P1 | P2 | P3 | P4 | P5 | P6 | P7 | P8 | P9 |
|---|---|---|---|---|---|---|---|---|---|
| (a) | 4.50 | 32.34 | 2.44 | 6.88 | 2.92 | 1.97 | 2.28 | 1.17 | 1.52 |
| (b) | 4.50 | 0 | 2.44 | 6.88 | 2.92 | 1.97 | 2.28 | 1.17 | 1.52 |
| (c) | 4.50 | 0 | 2.44 | 0 | 2.92 | 0 | 2.28 | 0 | 1.52 |
| (d) | 4.50 | 0 | 2.44 | 0 | 0 | 0 | 2.28 | 0 | 1.52 |

Second method: reduced influence coefficient matrix is used by excluding the points where gauges are not installed.

e) All nine gauges are installed

f) By excluding P2 gauge, the load is calculated using $[8 \times 8]$ reduced matrix

g) Load is calculated by $[5 \times 5]$ reduced matrix by excluding P2, P4, P6, and P8 gauges

h) Load is calculated by $[4 \times 4]$ reduced matrix by excluding P2, P4, P5, P6, and P8 gauges

The results for above eight cases are shown in Table 2-11 and Table 2-12. A load of 10 kgf is applied to P2 point in experiments. Fig. 2-22 shows the total force calculated by two methods. In both methods, as the number of points without gauge increases, the calculated load for each gauge increases slightly, but the total load decreases gradually when compared to actual value. The actual load is 106.82N and about 8% difference from the theoretical value of 98.1N. From this simple experiment, it can be concluded that the load calculated by the reduced influence coefficient matrix is closer to actual load than the load calculated assuming zero stresses. Therefore, the use of reduced influence coefficient matrix is recommended for the load inversion process.

Table 2-11 Calculated results of assuming stresses of the removed gauges as zero

| (unit : MPa) | P1 | P2 | P3 | P4 | P5 | P6 | P7 | P8 | P9 | Total load (N) |
|---|---|---|---|---|---|---|---|---|---|---|
| (a) | 8.14 | 97.78 | -0.12 | -4.30 | -0.42 | 1.21 | 3.75 | 0.18 | 0.60 | 106.82 |
| (b) | 15.56 | -2.45 | 7.30 | -0.76 | 6.39 | 4.74 | 6.72 | 1.65 | 3.51 | 42.72 |
| (c) | 16.04 | -1.97 | 8.20 | -2.99 | 7.23 | -2.14 | 7.36 | -1.54 | 4.63 | 34.81 |
| (d) | 16.78 | -1.47 | 8.94 | -2.32 | -1.09 | -1.47 | 8.11 | -1.04 | 5.37 | 31.82 |

Table 2-12 Calculated results using reduced matrix

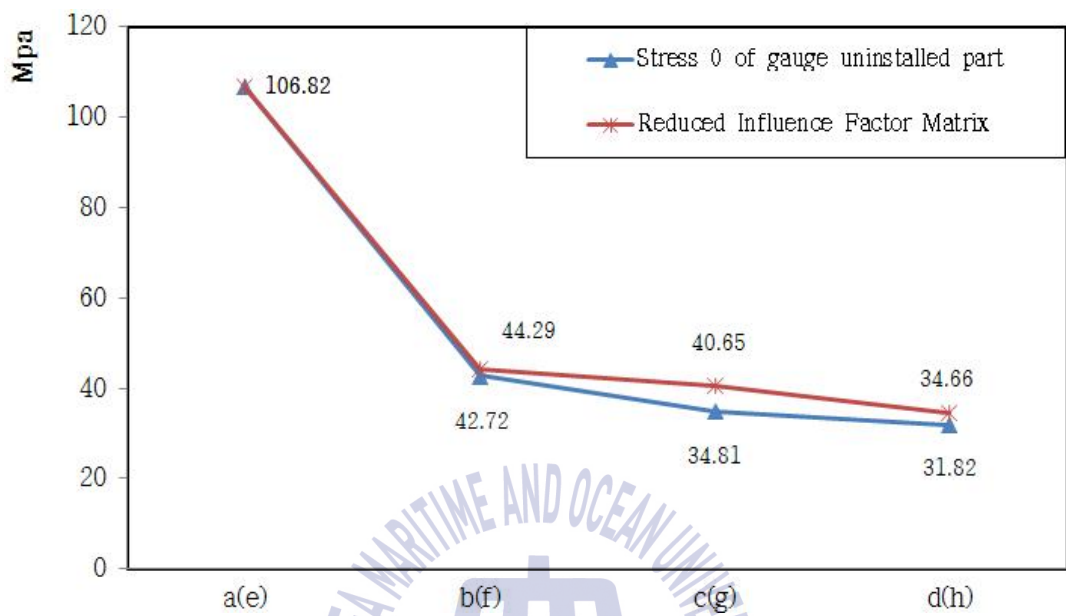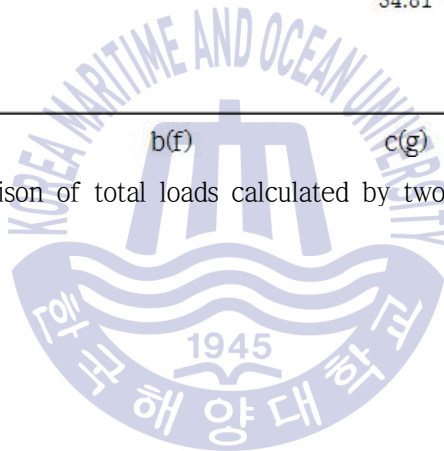| (unit : MPa) | P1 | P2 | P3 | P4 | P5 | P6 | P7 | P8 | P9 | Total load (N) |
|---|---|---|---|---|---|---|---|---|---|---|
| (e) | 8.14 | 97.78 | -0.12 | -4.30 | -0.42 | 1.21 | 3.75 | 0.18 | 0.60 | 106.82 |
| (f) | 15.38 | ? | 7.12 | -0.85 | 6.23 | 4.65 | 6.65 | 1.62 | 3.50 | 44.29 |
| (g) | 15.44 | ? | 7.68 | ? | 6.61 | ? | 6.79 | ? | 4.13 | 40.65 |
| (h) | 16.24 | ? | 8.48 | ? | ? | ? | 6.39 | ? | 3.55 | 34.66 |

Fig. 2-23 Comparison of total loads calculated by two different methods

# 3. Calculation of local ice loads from pressures acting on shell plating

## 3.1 Local ice load estimation procedure and the concept of collision events

This section describes the local ice pressures acting on the shell plating. Here, the ice pressure acting on shell plating means the sum of local pressures acting on each gauged sub-region in the shell plating. This local ice pressures/load act directly on the shell plating and its surrounding members and result in structural damage.

The procedure for calculating local ice load consists of various intermediate steps; First, von Mises equivalent stresses are calculated from the measured strain data in time domain. Instead of a continuous time series calculation, a concept of "collision events" was adopted in the analysis of stresses. A collision event is defined as the sequential time history of stresses from the beginning of ice contact with hull structure to the time of ice disconnection. When a big enough ice feature collides with the ship hull, the impact load increases sharply and the ship speed starts decreasing. At the end of ice-ship contact, the load drops and the ship speed regains. A maximum peak stress among many peak stresses inside one collision event can be selected. The next step is; maximum peak stresses are converted to ice pressures using the

influence coefficient method as described in the previous chapter. During a collision event, one max. peak hull stress and one max. peak ice pressure can be determined. Then by multiplying the ice pressure by the sub-region area where strain gauges are installed, a sum of max. peak ice pressures on the entire gauged shell plating can be obtained and it is called as the local ice load in this study. All the calculation procedures are done with MS Excel sheets.

Stress criteria for selecting collision events are set to 15MPa or higher for 2010 Arctic ice trials and 10MPa or higher for 2015 Arctic ice trials. The duration of the collision event varies from 3 seconds to 10 seconds as shown in Fig. 3-1 and Fig. 3-2. Fig. 3-2 is an enlarged view of a collision event shown in Fig. 3-1.
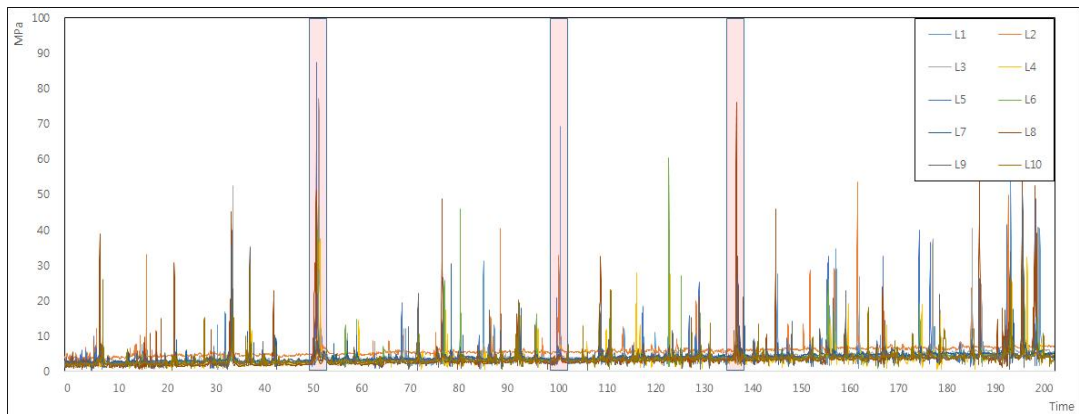
**Fig. 3-1** Hull stresses calculated from strain data and several collision events in time domain
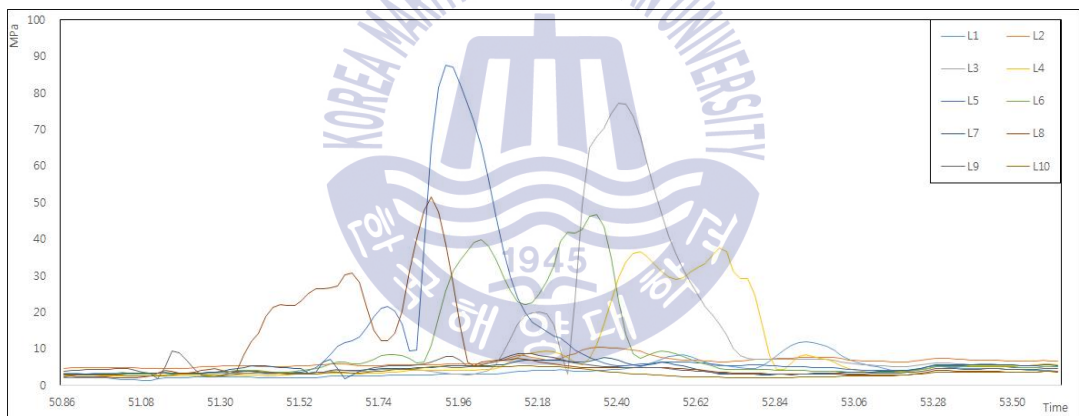


**Fig. 3-2** An enlarged view of a collision event section

## 3.2 Estimation of local ice loads from 2010 and 2015 Arctic ice trials

The Korean IBRV ARAON has conducted the ice trials in the Arctic and Antarctic seas five times in 2010, 2011, 2012, 2013 and in 2015 respectively. Table 3-1 summarizes the types of data acquired onboard ARAON during ice trials. The instruments used in the onboard measurements are strain gauges and a motion sensor. The local ice loads can be estimated using strain gauge data and the global ice load can be estimated with the measurement data from motion sensor. In the Table 3-1, *Official* means the official icebreaking test mode and *Transit* means general ice transit mode.

**Table 3-1** Types of data acquired onboard ARAON during ice trials

| Year | Region | Local Load (Strain gauges) | | Global Load (Motion sensor) | |
|------|--------|:--:|:--:|:--:|:--:|
| | | *Official* | *Transit* | *Official* | *Transit* |
| 2010 | Arctic | ○ | ○ | ○ | ○ |
| 2011 | Arctic | × | | ○ | ○ |
| 2012 | Antarctic | ○ | ○ | × | |
| 2013 | Arctic | × | ○ | × | |
| 2015 | Arctic | × | ○ | × | ○ |

In 2010 and 2015 Arctic ice trials, both strain gauges and motion sensor were used to collect ice load data during *Official* and/or *Transit* modes of icebreaking. In 2015 Arctic ice trials, instrumentation has been much improved since past several experiments. In this study, only 2010 (three official data sets recorded on August 4, 5, and 6) and 2015 (only 13 sets among 33 transit data sets) strain gauge data were analyzed since they reflects nearly same environmental conditions in the Arctic.

Fig. 3-3, and 3-4 show the statistical distribution of peak local ice loads in 2010 and 2015 tests, respectively. The local ice loads on gauged panel in 2010 are up to 1.1MN maximum and the average, 0.04MN and standard deviation, 0.03MN. Most frequent magnitude of local ice loads falls on 20kN ~ 40kN ranges. In 2015, the maximum load is 0.10MN, average 0.016MN and standard deviation 1.7kN. Most frequent magnitude of local ice loads falls on smaller than 1.0kN range, As seen from the figures the ice load measured in 2015 is much   smaller than that in 2010, which represents milder ice conditions in 2015 than in 2012.
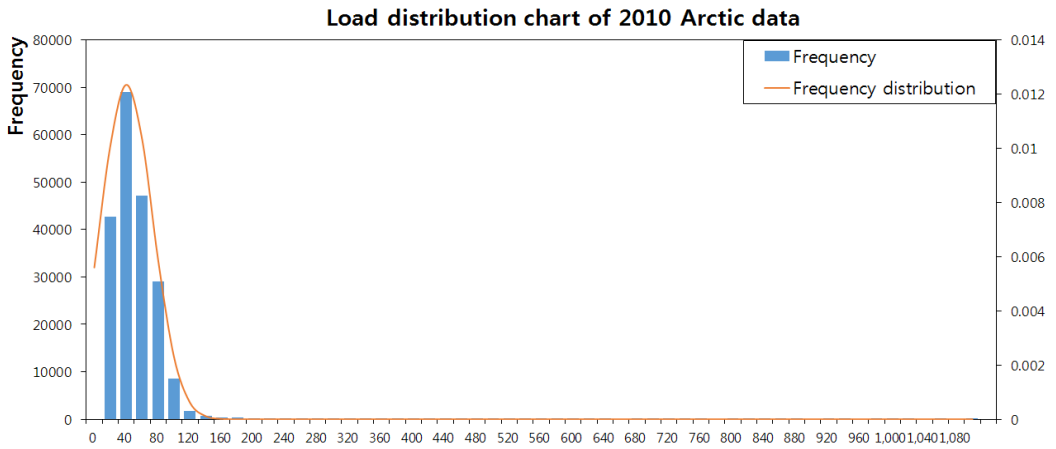
**Fig. 3-3** Distribution of peak local ice loads in 2010 tests
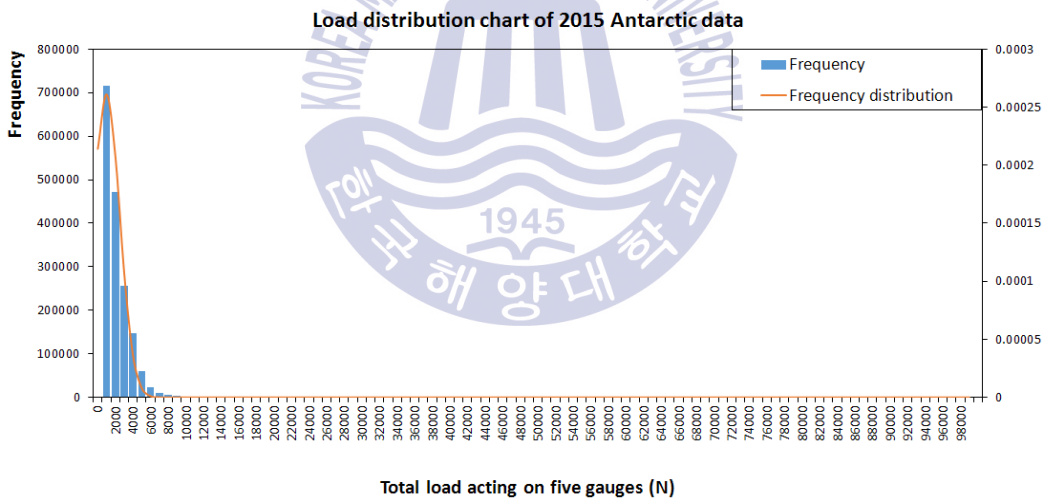


**Fig. 3-4** Distribution of peak local ice loads in 2015 tests

# 4. Calculation of local ice load by calculation of shear forces in hull frame

In 2015 Arctic ice trials, single gauges were installed inside the ARAON's shell plating to estimate the local ice loads. In addition, 3-axis rosette gauges were installed in the hull frames to compare with ice loads calculated from single gauge measurement in the shell plating. In this study, the local ice loads are estimated by calculating shear forces through the rosette gauges installed in hull frames.

The locations of rosette gauges installed in the hull frame are shown in Figs. 4-1 and 4-2. 10 rosette gauges were installed in four frames (Fr.106 ~ Fr.109) to port side and 4 rosette gauges in two frames (Fr.108 and Fr.109) to starboard side, as marked with circles in Figs. 4-1 and 4-2, respectively. Particularly, in Fr.108 port side, gauges were installed at both faces of the frame.
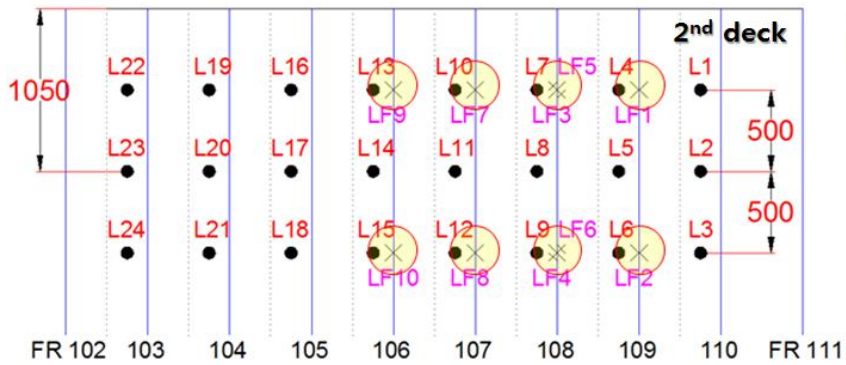
Fig. 4-1 Strain gauges installed on the hull frames in 2015 Arctic ice trials (port side)
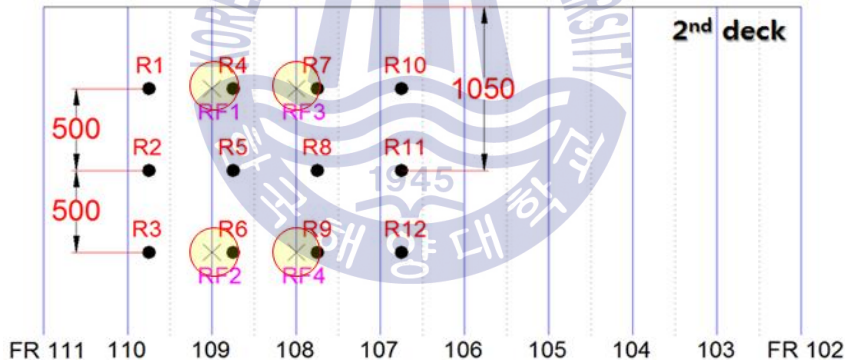


Fig. 4-2 Strain gauges installed on the hull frames in 2015 Arctic ice trial (starboard side)

Fig. 4-3 shows the strain gauges installed on the frame in detail. Two gauges were installed above and below the contact position of ice (i.e., waterline) on a hull frame. $\tau_1$ is the shear stress at the upper position and $\tau_2$ is shear stress at the lower position as shown in Fig. 4-3. Shaded area in Section A-A represents the shear area where the shear stresses are actually distributed over.
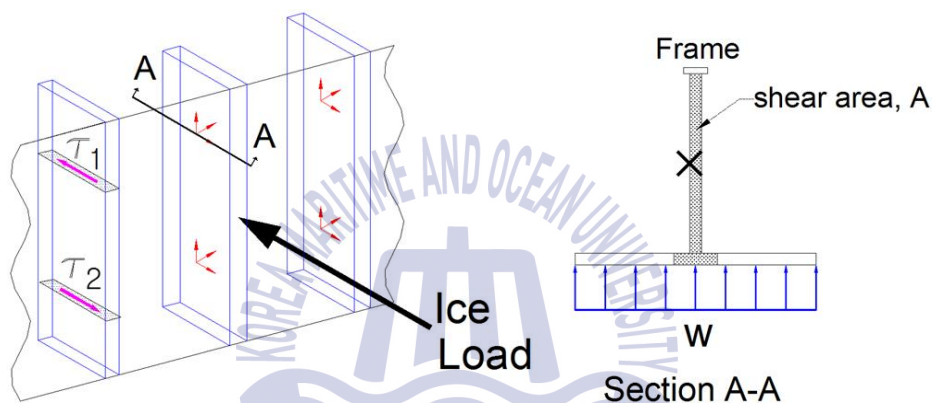


Fig. 4-3 A schematic diagram of the rosette gauge installed in the frame

Since the frame is solidly attached to shell plating, the frame-plating behaves together under the action of ice loads. The shear area shown in Fig. 4-3 can not represent actual section area where shear forces transmit. Therefore shear area should represent actual force-transmitting area which is the sum of frame cross section area and some part from shell plating area. The amount of additional area contributed from shell plating can be determined by effective width theory.

To deal with this problem, a frame with infinitely wide flange is considered as in Fig. 4-4. When the shell plating is subjected to bending, stress distribution becomes non-uniform and it can be assumed that only a part of the frame is fully loaded and no loads in the remaining part. Here $2\lambda$ is defined as the effective width. Effective width of a T-shaped beam is given by Eq.(5) (Timoshenko and Goodier, 1951)

$$2\lambda = \frac{4l}{\pi(3 + 2\nu - \nu^2)} \tag{5}$$

If Poisson ratio is 0.3, it becomes $2\lambda = 0.181 \times (2l)$. In other words, the effective width of the flange is approximately 18% of the span length. Since the interval between ARAON's frames is 0.8m, the effective width becomes 0.144m. Fig. 4-5 shows the cross section of the ARAON, where the strain gauge is installed.
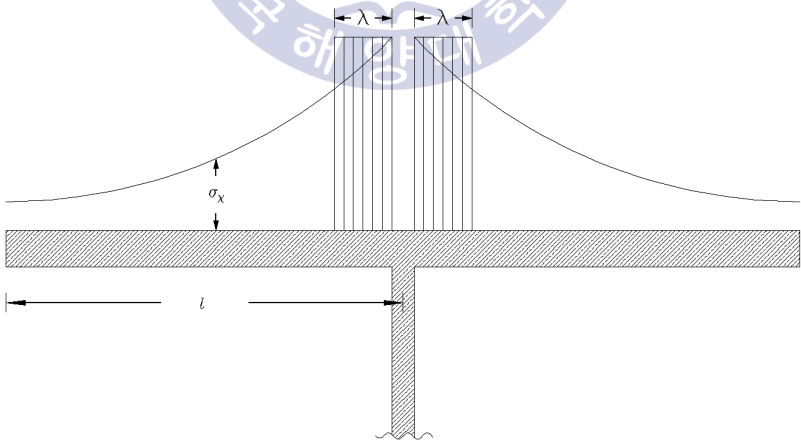


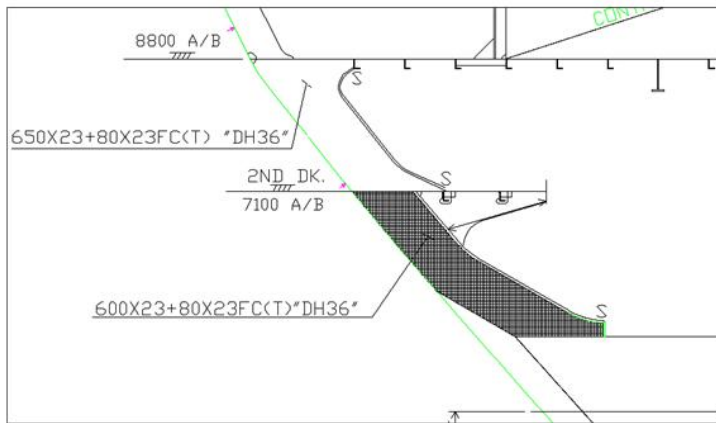**Fig. 4-4** A schematic diagram of a frame with infinitely wide flange

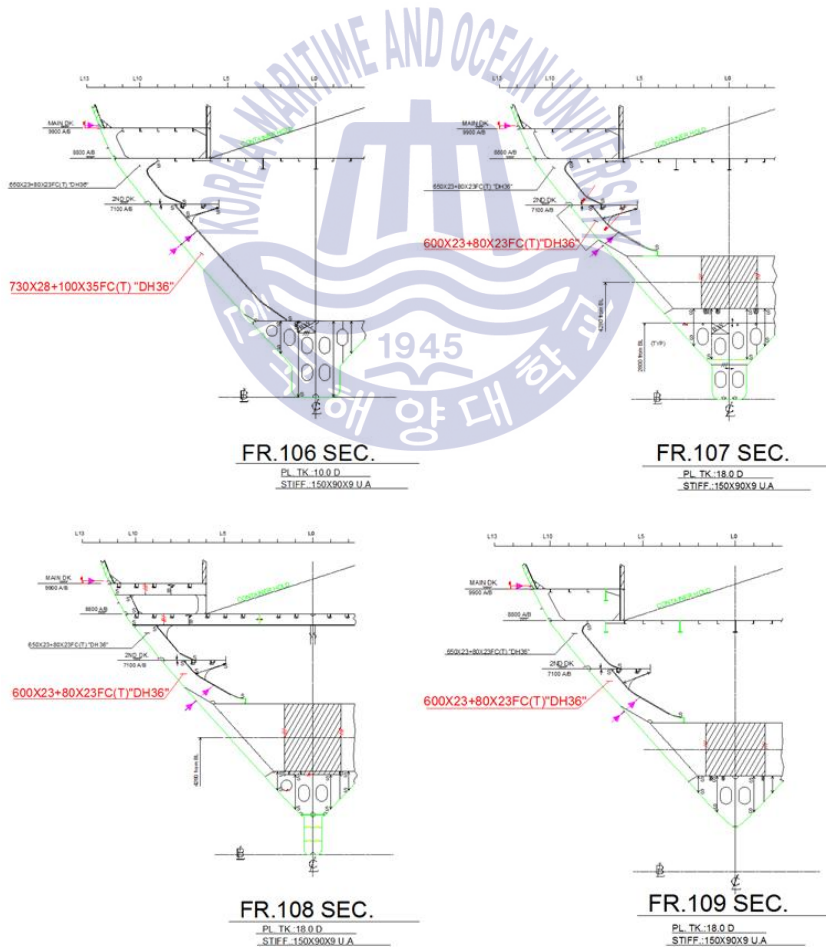**Fig. 4-5** Cross section of the ARAON where the strain gauge is installed



**Fig. 4-6** Cross-section of Fr.106~Fr.109

As shown in Fig. 4-6, since the cross-sectional area of No.106 frame of ARAON was designed different from that of No.107 ~ 109 frame, the actual area were calculated when The shear force acting on each frame is defined by Eq.(6).

$$F_{shear} = (\tau_1 - \tau_2)A \tag{6}$$

The shear stress $\tau$ is the product of shear modulus and shear strain. The elastic modulus E = 200GPa and the Poisson ratio $\nu$ = 0.3 are used in the calculation of shear stress.

$$\tau = G \cdot \gamma_a = \frac{E \cdot \gamma_a}{2(1+\nu)} \tag{7}$$

The 3-axis rosette gauge installed in hull frame measures normal strains $\epsilon_A, \epsilon_B, \epsilon_C$ in three directions. Mohr's circles and the shear strain is drawn as in Fig. 4-7 from three normal strains. Shear strain $\gamma_a$ is defined by Eq.(8) and the shear force transmitted to the frame can be calculated using Eq.(6).

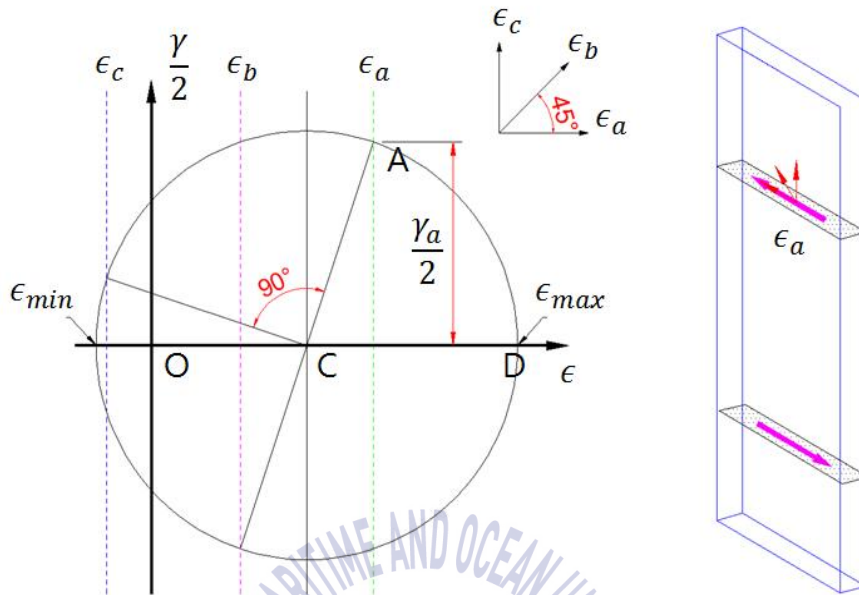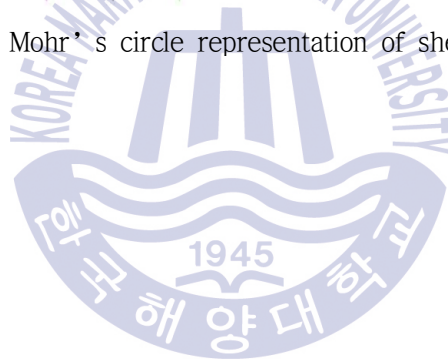$$\gamma_a = -(2\epsilon_b - \epsilon_a - \epsilon_c) \tag{8}$$

Fig. 4-7 Mohr's circle representation of shear strain

# 5. Comparison of ice load acting on shell plating and ice load in hull frame

   In 2015 Arctic ice trials, strain gauges were installed on the frame to measure shear strains for the first time in the series of annual ice field test. The purpose of this measurement was to compare local ice loads from the shear forces in the frame with those estimated from ice pressures on the shell plating. Previous researches have reported that ice loads could be estimated by using shear gauges on the hull frame of ships such as Manhattan, Canmar Kigoriak and Soya, but details of their procedures to analyze the measured data were not released (Mookhook et al., 1981; Ghoneim et al., 1984; Takimoto et al., 2006; Kujala et al., 2009; Suominen et al., 2013).

   Use of shear gauges in the hull frame can not only estimate local ice loads on small areas but also can estimate global ice load acting on entire ship structure by summing all shear forces in frames. However, in 2015 Arctic ice trials, the use of shear strain data was introduced as an alternative solution to estimate local ice load and the experimental setup was primitive. Only the shaded sections of data sets in Table 5-1 were analyzed. Data from L21 gauge could not retrieved because of gauge failure and data transient occurred in three data sets measured on August 10. In addition, data from L22 gauge were not retrieved on August 18, 19 and 20.

In this study, two different methods to estimate local ice loads from measured strain data were compared. Only the sub-region of the shell plating, where shear strains were measured by L4 to L15 and R4 to R9 gauges, was considered in the analysis to compare two methods each other. As mentioned above, the shear forces acting on hull frame were calculated using shear strain data and shear stress/force equations. Single gauges were used to estimate ice pressures on the shell plating. Hull stress were calculated by using von Mises equivalent stress formula and ice pressures were derived by using the influence coefficient method. And finally the local ice load can be calculated by multiplying corresponding area.

Table 5-1 Data sets recorded during the Arctic ice trials of ARAON in 2015

| NO. | DATE | UTC TIME | LATITUDE [N] | LONGITUDE [E] |
|---|---|---|---|---|
| 1 | | 11:30 ~ 12:50 | 79-00-34.848 / 79-12-57.150 | 172-49-32.070 / 172-43-54.870 [E] |
| 2 | 0810 | 14:20 ~ 16:20 | 79-27-35.658 / 79-44-09.888 | 172-37-43.902 / 172-21-00.972 [E] |
| 3 | | 16:25 ~ 18:00 | 79-44-48.156 / 79-59-44.562 | 172-21-02.988 / 172-21-14.412 [E] |
| 4 | | 00:05 ~ 02:00 | 80-05-10320 / 80-19-13.206 | 172-19-28.866 / 172-15-48.276 [E] |
| 5 | | 02:05 ~ 03:15 | 80-20-06.930 / 80-29-43.254 | 172-14-41.946 / 172-10-33.708 [E] |
| 6 | 0811 | 03:40 ~ 04:20 | 80-33-28.416 / 80-38-57.360 | 172-12-21.408 / 172-04-18.120 [E] |
| 7 | | 04:30 ~ 05:15 | 80-39-22.788 / 80-44-10.050 | 172-02-03.444 / 172-02-06.348 [E] |
| 8 | | 05:25 ~ 06:15 | 80-45-30.456 / 80-49-12.960 | 172-00-48.192 / 172-00-10.896 [E] |
| 9 | | 05:15 ~ 05:55 | 80-46-21.096 / 80-42-15.150 | 172-58-31.422 / 173-17-13.560 [E] |
| 10 | | 06:05 ~ 07:15 | 80-40-27.090 / 80-32-01.746 | 173-21-53.046 / 173-58-09.354 [E] |
| 11 | | 07:45 ~ 08:00 | 80-29-42.618 / 80-29-02.682 | 174-09-30.420 / 174-20-48.684 [E] |
| 12 | | 08:20 ~ 09:20 | 80-26-16.290 / 80-20-05.208 | 174-32-07.350 / 175-03-07.398 [E] |
| 13 | 0814 | 10:05 ~ 10:22 | 80-14-56.856 / 80-13-13.554 | 175-12-08.736 / 175-19-22.506 [E] |
| 14 | | 10:27 ~ 11:28 | 80-12-30.684 / 80-04-33.924 | 175-21-09.000 / 175-55-14.886 [E] |
| 15 | | 12:17 ~ 14:15 | 79-58-59.604 / 79-43-16.248 | 176-15-53.790 / 177-33-23.484 [E] |
| 16 | | 16:40 ~ 17:45 | 79-25-42.894 / 79-16-53.586 | 178-26-25.392 / 178-58-25.128 [E] |
| 17 | | 17:50 ~ 20:15 | 79-15-59.544 / 78-59-28.710 | 179-01-35.412 / 179-56-56.832 [E] |
| 18 | | 01:50 ~ 03:00 | 78-56-24.018 / 78-43-49.122 | 179-52-20.892 / 179-58-46.116 [W] |
| 19 | | 03:10 ~ 04:05 | 78-42-23.772 / 78-42-14.604 | 179-58-42.408 / 179-58-40.584 [W] |
| 20 | | 04:10 ~ 05:00 | 78-32-36.480 / 78-22-53.460 | 179-56-04.920 / 179-52-59.118 [W] |
| 21 | | 05:15 ~ 06:15 | 78-21-00.072 / 78-14-47.892 | 179-49-59.118 / 179-46-15.690 [W] |
| 22 | 0815 | 06:25 ~ 08:20 | 78-13-19.446 / 78-00-03.162 | 179-42-32.220 / 179-51-53.076 [W] |
| 23 | | 13:05 ~ 14:05 | 77-59-08.202 / 77-59-50.316 | 179-25-25.374 / 178-38-40.038 [W] |
| 24 | | 14:12 ~ 15:05 | 77-59-39.402 / 77-58-40.134 | 178-34-09.762 / 178-02-45.756 [W] |
| 25 | | 15:10 ~ 16:07 | 77-58-28.794 / 77-58-57.918 | 177-58-23.946 / 177-09-36.060 [W] |
| 26 | | 16:17 ~ 19:43 | 77-58-54.540 / 78-00-16.296 | 177-00-26.508 / 174-58-02.994 [W] |
| 27 | | 01:20 ~ 02:42 | 77-52-33.876 / 77-48-52.452 | 172-53-43.914 / 171-50-29.166 [W] |
| 28 | 0816 | 02:50 ~ 03:50 | 77-48-37.254 / 77-46-02.988 | 171-45-20.196 / 171-14-24.852 [W] |
| 29 | | 04:09 ~ 05:10 | 77-44-52.314 / 77-43-16.872 | 171-09-21.180 / 170-21-58.470 [W] |
| 30 | | 05:20 ~ 06:15 | 77-43-09.054 / 77-41-54.402 | 170-13-41.670 / 169-29-27.402 [W] |

Figs. 5-1 and 5-2 show the calculated shear forces for each frame and total sum of shear forces in time domain. Figs. 5-3 and 5-4 show the calculated ice loads on shell plating which corresponds to each frame and total sum of ice loads respectively.
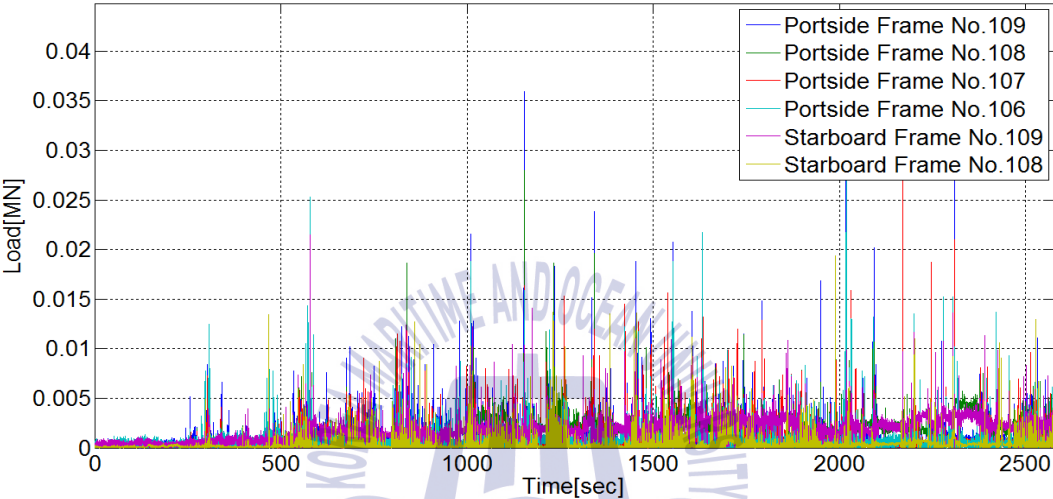


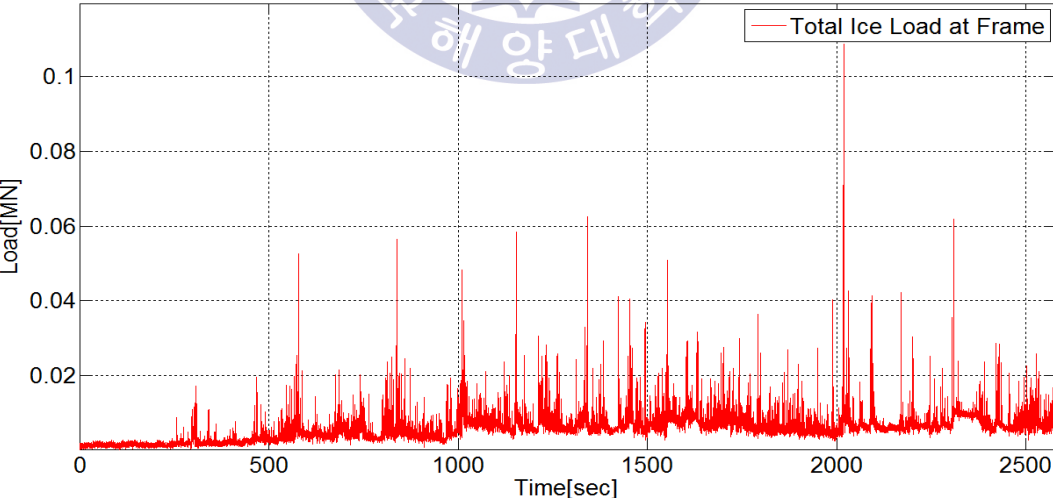Fig. 5-1 Calculated shear forces in each frame



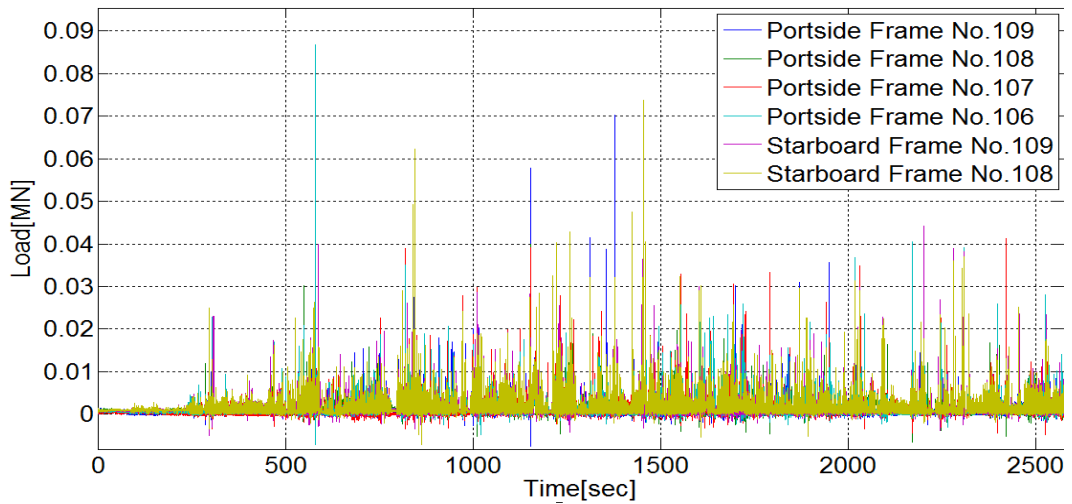Fig. 5-2 Sum of the shear forces acting on each frame

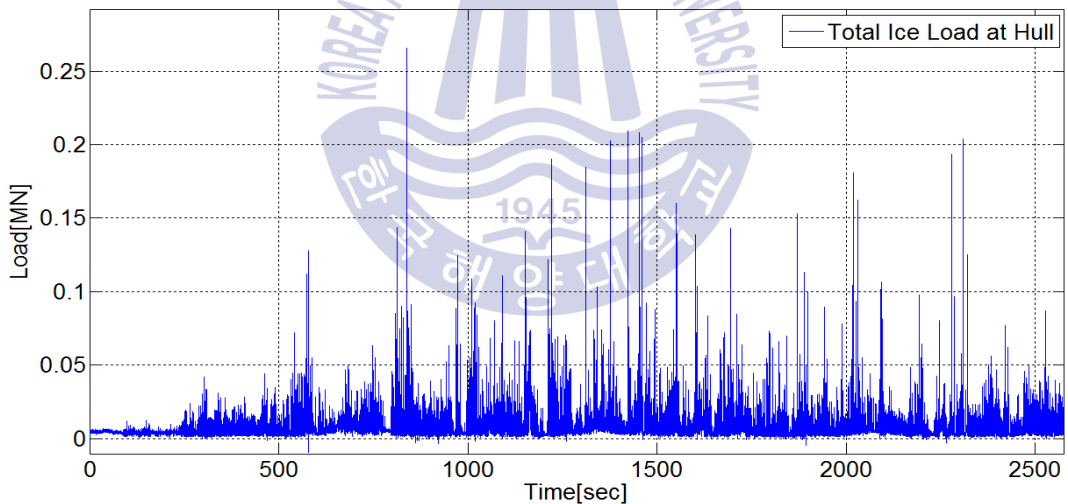**Fig 5-3** Calculated ice loads on shell plating corresponding to each frame



**Fig 5-4** Sum of the ice loads on shell plating

In comparison of two calculation methods, Fig. 5-5 shows the calculated local ice loads by two approaches. Fig. 5-6 shows an enlarged graph of calculated results around 839sec in Fig. 5-5. Generally the time of peak ice load in the shell plating is almost same as the time of peak ice load

- 50 -

calculated in hull frame. But in some other cases, the times of the peak ice loads showed a slight difference of 0.02sec to 3sec. Even though the gauges were installed symmetrically with respect to the center of the frame, the shear force histories at both faces were slightly different and the time difference of peak loads fall on between 0.02sec to 0.06sec as shown in Fig. 5-7 (Fr.108 for example). Anyway, if the peak ice loads occur within small time difference, sum of these ice loads can be treated as a local ice load in the same collision event.
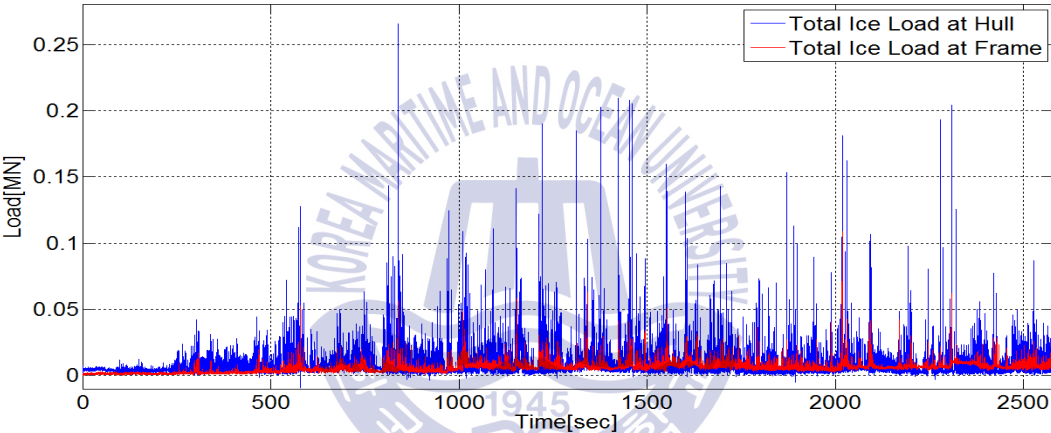


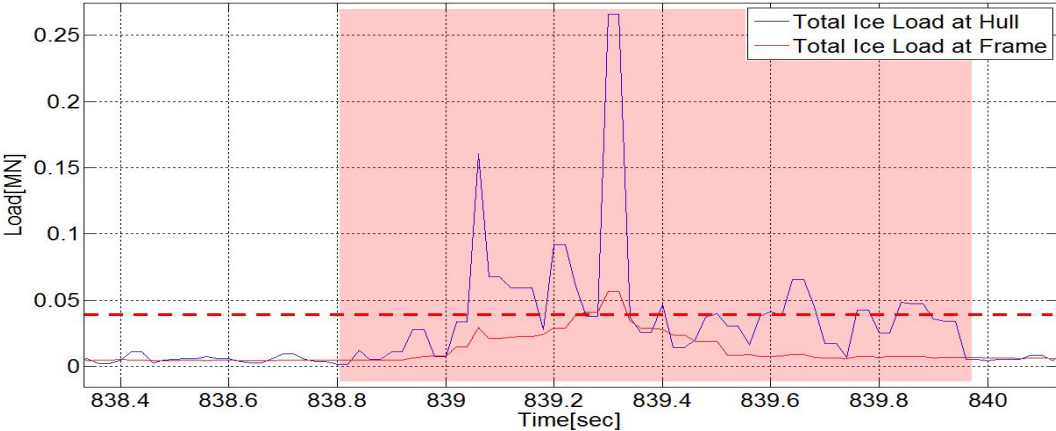Fig 5-5 Comparison of local ice loads calculated by two approaches



Fig 5-6 Comparison of two peak ice loads in an event section

**Table 5-2** Comparison of local ice loads in each event

| Data set No. | Time [sec] | Plate load [MN] | Frame load [MN] | Data set No. | Time [sec] | Plate load [MN] | Frame load [MN] |
|---|---|---|---|---|---|---|---|
| 7 | 579 | 0.08 | 0.05 | | 4544 | 0.11 | 0.05 |
| | 839 | 0.27 | 0.06 | | 5322 | 0.14 | 0.04 |
| | 1010 | 0.11 | 0.05 | | 5691 | 0.11 | 0.04 |
| | 1153 | 0.10 | 0.06 | | 6039 | 0.33 | 0.04 |
| | 1342 | 0.10 | 0.06 | | 6072 | 0.16 | 0.06 |
| | 1424 | 0.21 | 0.04 | | 6349 | 0.13 | 0.04 |
| | 4552 | 0.16 | 0.05 | | 6808 | 0.23 | 0.04 |
| | 1989 | 0.08 | 0.04 | | 8035 | 0.08 | 0.04 |
| | 2018 | 0.18 | 0.11 | 22 | 174 | 0.04 | 0.05 |
| | 2030 | 0.16 | 0.04 | | 998 | 0.06 | 0.04 |
| | 2093 | 0.11 | 0.04 | | 3328 | 0.05 | 0.07 |
| | 2170 | 0.05 | 0.04 | | 4045 | 0.07 | 0.05 |
| | 2309 | 0.20 | 0.06 | | 4194 | 0.08 | 0.06 |
| 14 | 2333 | 0.04 | 0.04 | | 4227 | 0.05 | 0.04 |
| | 2984 | 0.06 | 0.05 | | 4616 | 0.13 | 0.06 |
| | 3059 | 0.15 | 0.04 | | 4992 | 0.13 | 0.05 |
| 17 | 1370 | 0.24 | 0.04 | | 5642 | 0.17 | 0.06 |
| | 1637 | 0.14 | 0.05 | 23 | 790 | 0.05 | 0.05 |
| | 1712 | 0.10 | 0.04 | | 827 | 0.12 | 0.08 |
| | 3321 | 0.13 | 0.04 | | 2192 | 0.16 | 0.05 |
| | 3633 | 0.12 | 0.04 | 28 | 660 | 0.19 | 0.04 |
| | 3827 | 0.13 | 0.05 | | | | |

**Table 5-3** Estimated local ice loads calculated by two approaches

| | Plate load | Frame load |
|---|---|---|
| Event average | 0.13 MN | 0.05 MN |
| Event max. | 0.33 MN | 0.11 MN |

In this study, all the collision events were selected and the maximum values of two ice loads estimated within the event time were extracted (Table 5-4). Table 5-5 shows the average and maximum values of ice loads estimated for all collision events. Maximum value of the ice loads for all collision events in Table 5-4 was 0.33MN on the shell plating and 0.11MN in the hull frames. Average value of the ice loads were 0.13MN and 0.05MN, respectively. Estimated local ice load in frames from shear strain data was about 40% of the estimated ice load on the hull plating. Even though just a few numbers of strain gauges were used in the shear force estimation and the location of installed gauges was not properly selected, the comparison show some trends of ice loads calculated by two different methods and it needs to consider later on. Shear force calculation is directly affected by the measured shear strain $\gamma_a$. The position of the rosette gauge installed in 2015 Arctic ice trials was the center of frame width, assuming that the shear deformation at the cross section of the frame is uniform. If the gauge is installed closer to the hull plating, the shear deformation will be larger and it is expected that two results will be comparable.
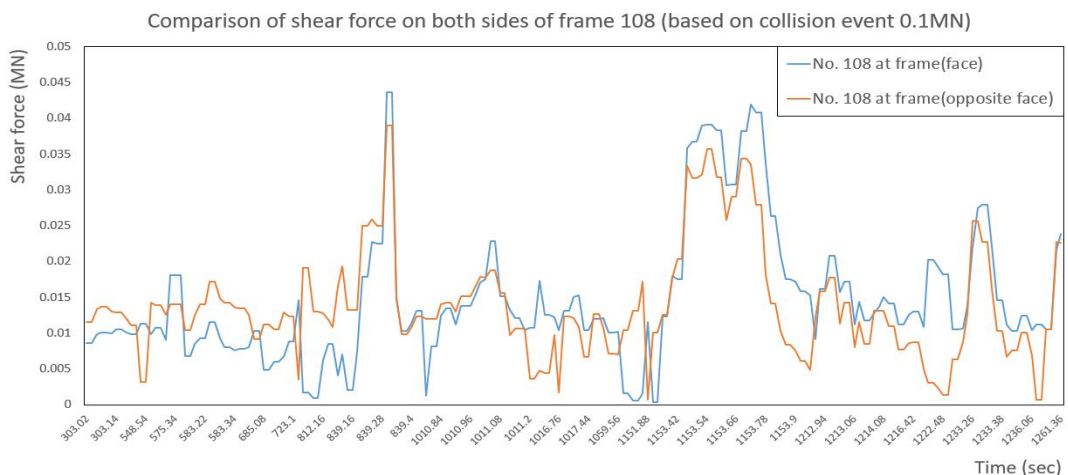


Fig. 5-7 Comparison of shear forces estimated on both sides of frame No.108

# 6. Conclusions

In this thesis, local ice loads were estimated from the analysis of strain gauge data installed on the shell plating and hull frames. To collect strain data during collision events, the Korean IBRV ARAON was used to perform ice trials during her 2015 Arctic voyage. The ice loads were calculated from shell plating pressures using an influence coefficient method.

Following conclusions can be drawn:

1) When single gauges are installed, an approach to calculate von Mises equivalent stress rather than using uniaxial Hooke's law is recommended.

2) Through the statistical analysis for gauge locations in 2010 and 2015 Arctic ice trials, it is found that interpolation method in vertical direction is better than in longitudinal direction. And the reduction of influence coefficient matrix gives more accurate values in calculating stresses.

3) Local ice loads can be calculated by summing shear forces acting on frames or ice pressures acting on shell plating. The estimation of local ice loads calculated by two different methods were compared to each other. It was shown that the frame ice load was about 40% of shell plating ice load. As a result, the alternate approach for estimating local ice loads from shear strain measurement is recommended. Load-stress relationship, Eq.(6) can be modified as follows:

$$F_{shear} = K(\tau_1 - \tau_2)A \tag{9}$$

where coefficient $K$ is a parameter that relates shear forces to shear stresses and later it should be determined through field ice trial data.

# References

Choi, K.S.,, 2015. *Ice Loads on Icebreaking Vessels*, Munundang.

Choi, K.S., Jeong, S.Y., 2008. *Ice Load Prediction Formulas for Icebreaking Cargo Vessels, Journal of the Society of Naval Architects of Korea*, 45(2), pp.603-610

Cheon, E.J., Choi, K.S., Kim, H.Y.,  & Lee, T.K., 2014. Analysis of Strain Gauge Data Onboard the IBRV ARAON during Icebreaking Voyage in the Antarctic Sea Ice, *Journal of the Society of Naval Architects of Korea*, 40(6), pp.489-494.

Ghoneim, G.A.M., Johansson, B.M., Smyth, M.W., & Grinstead, J., 1984. Global Ship Ice Impact Forces Determined from Full-scale Tests and Analytical Modeling of the Icebreakers Canmar Kigoriak and Robert LeMeur. *Society of Naval Architects and Marime Engineers Transactions*, 92, pp.253-282.

Kim, H.Y., 2014. *Analysis of Strain Gauge Data and Estimation of Ice Load on the IBRV ARAON in the Antarctic Sea*, Master's thesis, Busan: Korea Maritime and Ocean University.

Kujala, P., Suominen, M., & Riska, K., 2009. Statistics of Ice Loads Measured on MT UIKKU in the Baltic. *Proceedings of the 20$^{th}$ International Conference on Port and Ocean Engineering under Arctic Conditions*, Lulea Swden, pp.810-823.

Kwon, Y.H., Choi, K.S., & Lee, T.K., 2015. A Study on Statistical Analysis of Local Ice Loads Measured during the Arctic Voyage of the IBRV ARAON. *Poceedings of the Twenty-fifth International Ocean and Polar Engineering Conference*, Hawaii USA.

Lee, T.K., Kim, T.W., Rim, C.W., & Kim, S.C., 2013. A Study on Calculation of Local Ice Pressures for ARAON Based on Data Measured at Arctic Sea, *Journal of Ocean Engineering and Technology*, 27(5), pp.88-92.

Suominen, M., et al., 2013. Full-sacle Measurements on Board PSRV S.A. AGULHAS II in the Baltic Sea. *Proceedings of the 22<sup>th</sup> International Conference on Port and Ocean Engineering under Arctic Conditions*, Espoo Finland.

Timoshenko, S.P., and Goodier, J.N., 1951. *Theory of Elasticity*. 3nd, McGraw Hill Education: New York.

Takimoto, T., et al., 2006. Measurement of Ice Load Exerted on the Hull of Icebreaker SOYA in the Southern Sea of Okhotsk. *Proceedings on the 18<sup>th</sup> IAHR International Symposium on Ice*, Sapporo Japan, (2), pp.41-48.

Yang, Y.K., 2012. *Sports Statistics*, Yidam-Books: Seoul.